Electronic structure of *d*-wave superconducting quantum wires

A. M. Bobkov,[1,2] L.-Y. Zhu,[3] S.-W. Tsai,[3,4] T. S. Nunner,[3] Yu. S. Barash,[1,2] and P. J. Hirschfeld[3]
[1]*Lebedev Physical Institute, Leninsky Prospect 53, Moscow 119991, Russia*
[2]*Institute of Solid State Physics, Chernogolovka, Moscow Region 142432, Russia*
[3]*Department of Physics, University of Florida, Gainesville, Florida 32611, USA*
[4]*Department of Physics, Boston University, Boston, Massachusetts 02215, USA*
(Received 24 February 2004; revised manuscript received 3 May 2004; published 7 October 2004)

We present analytical and numerical results for the electronic spectra of wires of a *d*-wave superconductor on a square lattice. The spectra of Andreev and other quasiparticle states, as well as the spatial and particle-hole structures of their wave functions, depend on interference effects caused by the presence of the surfaces and are qualitatively different for half-filled wires with even or odd number of chains. For half-filled wires with an odd number of chains N at (110) orientation, spectra consist of N doubly degenerate branches. By contrast, for even N wires, these levels are split, and all quasiparticle states, even the ones lying above the maximal gap, have the characteristic properties of Andreev bound states. These Andreev states above the gap can be interpreted as a consequence of an infinite sequence of Andreev reflections experienced by quasiparticles along their trajectories bounded by the surfaces of the wire. Our microscopic results for the local density of states display atomic-scale Friedel oscillations due to the presence of the surfaces, which should be observable by scanning tunneling microscopy. For narrow wires the self-consistent treatment of the order parameter is found to play a crucial role. In particular, we find that for small wire widths the finite geometry may drive strong fluctuations or even stabilize exotic quasi-one-dimensional pair states with spin-triplet character.

DOI: 10.1103/PhysRevB.70.144502 PACS number(s): 74.45.+c, 74.78.Na, 74.81.−g

I. INTRODUCTION

Since the discovery of high-temperature superconductivity (HTS), the origin of the pairing phenomenon in these materials has been the subject of intense debate, and is still not clarified. Part of the unusual nature of HTS which has hindered theoretical analysis is the short coherence length, which allows short-wavelength fluctuations of various types of local order to coexist with superconductivity. Most probes of the nature of the superconducting state have been restricted, until fairly recently, to measurements of bulk properties and tunneling through relatively large areas. Following the pioneering work of Hess *et al.*,[1] it was realized that scanning tunneling microscopy (STM) could provide an atomic-scale picture of the superconducting state, particularly useful when applied to inhomogeneous situations such as the vortex lattice. Measurements of this type were subsequently performed on high-temperature superconductors.[2] In the past few years, scanning tunneling microscopy on the surface of HTS have compiled a novel and fascinating picture of the local electronic structure of a few of these materials.[3–10] In the $Ba_2Sr_2CaCu_2O_8$ system (BSCCO), one dramatic implication of these experiments is that even relatively high quality single crystals display inhomogeneous electronic structure at the nanoscale.[7–10]

In parallel to studies of the HTS materials, point-contact spectroscopy has been used to study the electronic structure of ultrasmall conventional superconducting islands.[11] Among many fascinating consequences of the nanoscale geometry are number parity effects, in which the qualitative electronic structure depends sensitively on whether the number of electrons on the island are even or odd. More recently, superconducting wires of widths tens of nanometers[12] have also been fabricated. Although they have not yet been studied by STM or similar methods, this should be technically feasible.

Isolated nanoscale grains and wires of HTS material have not been fabricated to our knowledge. While this may prove technically quite difficult to achieve due to the complexity of the crystal structure, there seems to be no fundamental obstacle in the long run. This applies as well to other superconductors thought to manifest unconventional superconducting order, where effects of finite geometry should be easier to see since coherence lengths tend to be larger.

It is our purpose in this paper to study how *d*-wave (e.g., HTS) and other unconventional symmetry superconductors behave in finite geometry at the atomic scale. Ziegler *et al.*[13] began the study of this problem in the case of (100) *d*-wave quantum wires, pointing out the dependence of the Fermi-level density of states on the parity of the wire width. This is a natural consequence of the discretization of the electronic energy levels due to the finite wire width in the *d*-wave state. While in the *s*-wave case all the interesting physics is tuned by the level discretization, one expects *a priori* one fundamental difference in the *d*-wave case. For any geometry with surfaces making an arbitrary angle with the crystal axes, pair-breaking processes take place on a scale of the coherence length. The most important consequence for the electronic structure should be the formation of Andreev surface states.

However, little is known about how Andreev surface states behave when the size of the superconductor becomes comparable to ξ_0. The zero-energy states form on surfaces with orientations different from the antinodal directions of a *d*-wave superconductor, due to the sign change of the order parameter. In high-temperature superconductors, such states manifest themselves as the zero-bias conductance peak in tunneling spectroscopy in the *ab* plane,[14–39] the anomalous temperature behavior of the Josephson critical current[40–43]

and the upturn in the temperature dependence of the magnetic penetration depth[44–46] (see also review articles, Refs. 47,48). The conventional description of Andreev surface states, as well as the Andreev reflection itself, is based on the quasiclassical approximation, a powerful tool in the theoretical study of various properties of inhomogeneous superconducting systems.

The quasiclassical theory of superconductivity gives a so-called coarse-grained description of the phenomena, averaged over interatomic distances. This has been used, for example, to calculate the local quasiparticle density of states (LDOS). However, these coarse-grained averaged results are not adequate to analyze atomic resolution measurements by STM and some other contemporary experimental techniques (e.g., atomic force microscopy[49]). To obtain this type of information, a fully quantum-mechanical atomic-scale approach going beyond the quasiclassical approximation in describing inhomogeneous states of superconductors is required. We address this problem in the present paper using a tight-binding BCS-like model of a *d*-wave superconductor on a square lattice.

As a first step towards understanding the effect of constrained geometry, we study the simplest case of *d*-wave superconducting wires consisting of N parallel chains as the system size is reduced. The quasiparticle spectrum of such systems is described both analytically, with an assumed spatially homogeneous order parameter, and also numerically with a fully self-consistent approach. In the limit $N \gg 1$ the usual surface Andreev states in lattice models,[34,36,47] as well as the surface states known in continuous models,[23] can be recovered at each surface of the wire. However, for sufficiently narrow wires, when the transverse wire dimension is the order of the superconducting coherence length, the Andreev states strongly interfere and give rise to qualitatively new effects. We show below that only those effects which occur for bands sufficiently far from half filling and relatively wide wires can be described with the quasiclassical theory of superconductivity. In addition, we demonstrate how and under what conditions one can recover earlier quasiclassical results for Andreev states in *d*-wave superconducting films[50] from our microscopic approach.

The microscopic method adopted in this paper to constrain the geometry involves introducing lines of impurities of potential strength taken to infinity to bound the wire. We show that earlier microscopic results on (110) surfaces[23,34,36,47,51] and (100) wires[13] can be reproduced by this technique, and then extend it to calculate results on wires with other orientations. We find that the results for electronic spectra are very sensitive to the number parity of the wire width, and that true zero-energy Andreev states can only exist in wires with odd numbers of chains. In even wires, the Andreev states are split, pushed away from the Fermi energy, and can have either surface or standing wave character. Finally, we show that for smaller wires self-consistency effects become important and can even, within mean-field theory, lead to condensation of a fully gapped spin-triplet state instead of *d*-wave order.

Our results may also have some qualitative relevance for the related problem of *d*-wave superconducting grains, where the geometry is constrained in two dimensions. In addition to artificially fabricated islands, some authors have proposed that the BSCCO-2212 samples which display nanoscale inhomogeneity should be thought of as a collection of weakly coupled *d*-wave grains of roughly the size of the superconducting coherence length ξ_0, or *d*-wave grains coupled to grains of another electronic phase.[7,9,10,52] In fact, the structure of a general, possibly irregular small grain of *d*-wave superconductor, has not been studied to our knowledge. Understanding how the LDOS of these wires depend on the wire width and the orientation, as well as on the deviation from half filling, could provide important intuition for the question of the electronic structure of the small irregular grains possibly present in BSCCO samples.

The outline of the paper is as follows. In Sec. II, we introduce the formalism for the problem. In Sec. III, we discuss three special semi-infinite surface orientations: (110), (210), and (100). In Sec. IV B 2, we study the (110) superconducting wires with even and odd width and make a comparison with the discrete states in normal metal wires (Sec. IV B 1) to try to identify the nature of the true Andreev states. In Sec. IV B 3, we study the effects of deviations from the half filling. In Sec. V the results of fully self-consistent calculations are presented. In particular, we allow the order parameter to vary spatially and comment on the differences in our results. In the case of narrow wires the self-consistent study shows the appearance of some peculiar types of superconducting pairing. Finally, in Sec. VI, we present our conclusions.

II. MODEL DESCRIPTION AND FORMALISM

The Hamiltonian for a pure singlet superconductor can be written as

$$\mathcal{H} = -t \sum_{\langle i,j\rangle,\sigma} c^{\dagger}_{i\sigma} c_{j\sigma} - \sum_{i,\sigma} [\mu - U_i] c^{\dagger}_{i\sigma} c_{i\sigma} + \sum_{\langle i,j\rangle} \{\Delta_{ij} c^{\dagger}_{i\uparrow} c^{\dagger}_{j\downarrow} + \text{H.c.}\}, \tag{1}$$

where we have chosen a nearest-neighbor tight-binding band for simplicity; μ is the chemical potential. A superconducting pairing is defined for nearest neighbors $\Delta_{ij} = -V\langle c_{j\downarrow} c_{i\uparrow}\rangle$ on the bond $\{i,j\}$. The parameter t is of order 150 meV for high-T_c materials, and we consider both the particle-hole symmetric model $\mu = 0$ and the more realistic case of finite μ. In non-self-consistent calculations the order parameter has the familiar k-space form $\Delta_{\mathbf{k}} = \Delta_0[\cos(k_a a) - \cos(k_b a)]$, where $\Delta_0 = \frac{1}{2}\Sigma_{\pm}(\Delta_{ii\pm r_a} - \Delta_{ii\pm r_b})$ is independent of i, and is taken to be $0.2t$. The lattice constant is denoted by a. The maximum gap is $\Delta_{\max} = 2\Delta_0$. We also present self-consistent calculations, in which case V is chosen to yield this same value of Δ_0 far from wire edges.

It is possible to constrain the geometry underlying Eq. (1) in several different ways. We present results here for a method discussed, for example, in Refs. 34,53 in which the on-site potentials U_i are chosen to lie on the boundary and their value is taken to infinity to cut off electron transport through the boundary. This technique has the virtue that the strength of the barrier can in principle be lowered to allow different degrees of transparency and the study of tunneling

phenomena. In this work we restrict ourselves to impurity configurations and strengths for which the constrained system is completely isolated from its environment. This is equivalent to the assumption of open boundaries, when no hopping and no pairing take place outside the region. No disorder is introduced in the system and we consider U_i as "impurity" potentials only so as to form the surfaces of the superconducting region.

The Hamiltonian of the surface term is taken to be

$$U = U_0 \sum_{\ell\sigma} c^{\dagger}_{\ell\sigma} c_{\ell\sigma}, \tag{2}$$

where the set of sites ℓ is determined exclusively by the boundaries of the desired system (see below). The full Fourier space Green's function for the system in the presence of these impurities is quite generally

$$\check{G}(\mathbf{k},\mathbf{k}',\omega) = \check{G}^{(0)}(\mathbf{k},\omega)\delta_{\mathbf{k},\mathbf{k}'} + \check{G}^{(0)}(\mathbf{k},\omega)\check{T}(\mathbf{k},\mathbf{k}',\omega) \times \check{G}^{(0)}(\mathbf{k}',\omega), \tag{3}$$

where the T matrix can be found from the following equations:

$$\check{T}(\mathbf{k},\mathbf{k}',\omega) = \check{U}(\mathbf{k},\mathbf{k}') + \sum_{\mathbf{k}''} \check{U}(\mathbf{k},\mathbf{k}'')\check{G}^{(0)}(\mathbf{k}'',\omega)\check{T}(\mathbf{k}'',\mathbf{k}',\omega). \tag{4}$$

Here $\check{G}$ and $\check{T}$ take 4×4 matrix form in the four-dimensional product space of particle-hole and spin variables. If we choose nonmagnetic on-site potentials and consider singlet superconductors, the problem reduces to 2×2 matrices in Nambu space. The Nambu retarded propagator for the pure *d*-wave superconductor is

$$\hat{G}^{(0)}(\mathbf{k},\omega) = \frac{\omega\hat{\tau}_0 + \xi_{\mathbf{k}}\hat{\tau}_3 + \Delta_{\mathbf{k}}\hat{\tau}_1}{(\omega + i0)^2 - \xi^2_{\mathbf{k}} - \Delta^2_{\mathbf{k}}}, \tag{5}$$

where the τ_α are the Pauli matrices and $\xi_{\mathbf{k}} = -2t[\cos(k_a a) + \cos(k_b a)] - \mu$. Calculating the T matrix allows us to obtain the eigenenergies of the system from the condition $\det\hat{T}^{-1}(\omega) = 0$.

The local spin-resolved quasiparticle density of states is given as

$$\rho_{\uparrow(\downarrow)}(\mathbf{r},\omega) = -\pi^{-1}\mathrm{Im}\, G_{11,\uparrow\uparrow(\downarrow\downarrow)}(\mathbf{r},\mathbf{r},\omega). \tag{6}$$

After integration of the LDOS over energy, we should obtain the total number of quasiparticle states for each site. Since each site on the lattice possesses two states with opposite spins, the spin-resolved LDOS normalization is

$$\int_{-\infty}^{\infty} d\omega \rho_{\uparrow(\downarrow)}(\mathbf{r},\omega) = 1. \tag{7}$$

III. SURFACE CASE

Upon a conventional reflection on the (110) surface of a *d*-wave superconductor, the order parameter always changes sign as the direction of the quasiparticle momentum $\mathbf{k}$ is varied. This leads to Andreev reflection and, eventually, to the formation of the dispersionless zero-energy surface Andreev bound states. For other surface orientations the sign change does not take place for all incoming momentum directions. It is important to notice that the number of consecutive impurity lines that are needed in order to cut the system depends on the orientation of the surface one wants to consider. For (100) and (110) surfaces and nearest-neighbor hopping, one line of impurities is sufficient to cut communication between the two sides. For a (210) surface, the nearest-neighbor hopping and pairing terms can still connect this particle with another across a single line of impurities, so for a simple tight-binding band, two consecutive lines are needed to close the system (Fig. 1). Alternatively, if one includes a next-nearest-neighbor hopping t', even a (110) surface is not closed by a single line of infinite impurities; the system considered in Ref. 53 is therefore not a closed (impenetrable) surface. For a $(hl0)$ surface in general, $\max(h,l)$ lines are needed for a model that includes nearest-neighbor terms only, and $h+l$ lines are needed for a model that includes next-nearest-neighbor terms. Clearly, the technique becomes cumbersome for arbitrary angles, but one can nevertheless learn a good deal by considering special cases.

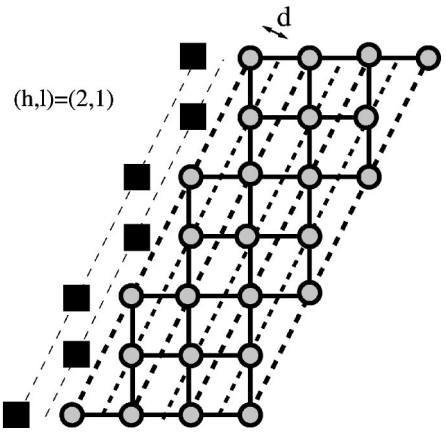

FIG. 1. (210) surface or wire. Two lines of impurities (closed squares) are needed to isolate the lattice sites (closed circles) with nearest-neighbor hopping.

In the presence of a surface of arbitrary orientation, the simplest way of applying Bloch's theorem to this discrete system is by using a surface-adapted Brillouin zone.[36,51] We define new coordinates $(\hat{x},\hat{y})$, rotated with respect to the crystal axes $(\hat{a},\hat{b})$, where $\hat{x}$ is the direction normal to the surface and $\hat{y}$ is the direction along the surface. The system is periodic along the y direction and the crystal momentum component k_y of a quasiparticle is conserved. Instead of the usual square Brillouin zone $k_a = [-\pi,\pi], k_b = [-\pi,\pi]$ (for unit lattice constant $a=1$) we now use the surface-adapted Brillouin zone given by $k_x = [-\pi/d, \pi/d]$ and $k_y = [-\pi d, \pi d]$. Here $d = 1/\sqrt{h^2+l^2}$ is the distance between the nearest chains (layers) aligned along the surfaces. The momenta in the two coordinate systems are simply related through rotation of an angle $\theta = \tan^{-1} h/l$.

Now we turn to the solution of the equation for the T matrix [Eq. (4)] for the case of one line of impurities. We start with the ansatz

$$\hat{T} = T_0\hat{\tau}_0 + T_1\hat{\tau}_1 + T_3\hat{\tau}_3 \tag{8}$$

and find, for arbitrary strength of impurity potential,

$$T_0(k_y,\omega) = \frac{G_0^{(0)}(0,k_y,\omega)}{D_1}, \tag{9}$$

$$T_1(k_y,\omega) = \frac{-G_1^{(0)}(0,k_y,\omega)}{D_1}, \tag{10}$$

$$T_3(k_y,\omega) = \frac{c - G_3^{(0)}(0,k_y,\omega)}{D_1}, \tag{11}$$

where $D_1(k_y,\omega)=[c-G_3^{(0)}(0,k_y,\omega)]^2-G_0^{(0)}(0,k_y,\omega)^2+G_1^{(0)}(0,k_y,\omega)^2, c=1/V_0$, and $G_i^{(0)}(x,k_y,\omega)$ is the Fourier transform with respect to k_x of the ith Nambu component of the bare Green's function $G_i^{(0)}(\mathbf{k},\omega)$

$$G_i^{(0)}(n,k_y,\omega) = \frac{d}{2\pi}\int_{k_x=-\pi/d}^{\pi/d} G_i^{(0)}(k_x,k_y,\omega)e^{ik_x nd}dk_x. \tag{12}$$

The site index n corresponds to x-coordinate $x=nd$. For the case of infinitely strong impurity potential considered here, $c=0$. In this case the expression for $\hat{T}$ can be written in the compact form,

$$\hat{T}(k_y,\omega) = -[\hat{G}^{(0)}(0,k_y,\omega)]^{-1}, \tag{13}$$

and the poles of the T matrix correspond to zeros of the determinant of the Green's function $\hat{G}^{(0)}(0,k_y,\omega)$.

The Fourier transform with respect to k_x of Eq. (3) is

$$\hat{G}(n,n',k_y,\omega) = \hat{G}^{(0)}(n-n',k_y,\omega) - \hat{G}^{(0)}(n,k_y,\omega) \times[\hat{G}^{(0)}(0,k_y,\omega)]^{-1}\hat{G}^{(0)}(-n',k_y,\omega). \tag{14}$$

Due to periodicity of the system along the y direction, calculation of the LDOS at site n will simply involve a sum of $G(n,n,k_y,\omega)$ over all values of k_y within the surface-adapted Brillouin zone and over two spin directions:

$$\rho(\mathbf{r},\omega) = \rho(n,\omega) = -\frac{2}{\pi}\mathrm{Im}\int_{-\pi d}^{\pi d}\frac{dk_y}{2\pi d}G_{11}(n,n,k_y,\omega). \tag{15}$$

A. (100) surface

Since (100) surfaces are not pair breaking in d-wave superconductors, we do not *a priori* expect to see interesting physics arising from Andreev states. On the other hand, the mere presence of a surface can induce surface Tamm bands,[54] decaying in the bulk on the atomic scale and experiencing the Friedel-like oscillations of the LDOS. In our model Tamm states have nothing to do with the superconductivity, although the possibility for pairing of electrons occupying these surface states is not excluded.[55] While it is not our intent to study these in detail, we present some results to show that such states can be seen by the STM even in situations where surface Andreev states are absent. Figure 2 shows on upper and lower panels the LDOS for various distances from the surface in the normal metal and the superconducting states, respectively.

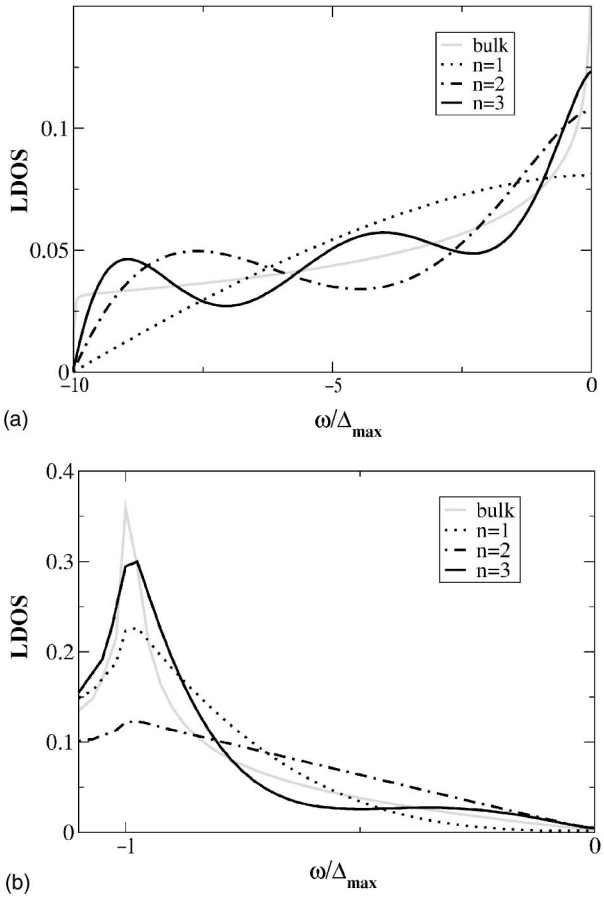

FIG. 2. Local density of states $\rho(x,\omega)$ for a (100) surface. Normal state (upper panel) and superconducting state (lower panel), $\rho(x,\omega)$ vs $\omega/\Delta_{\max}$ for various distances $n=x/d$ from surface; $\Delta_{\max}=0.4t, \mu=0$.

B. (110) surface

Results for a (110) surface are expected to be qualitatively different from the ones obtained for a (100) surface. The bulk order parameter in the coordinate system of the crystal axes $\hat{a}$ and $\hat{b}$ is $\Delta_{\mathbf{k}}=\Delta_0(\cos k_x a-\cos k_y a)$, but in the coordinates of the surface $\hat{x}$ (perpendicular to surface) and $\hat{y}$ (parallel to surface) becomes $\Delta_{\mathbf{k}}=2\Delta_0 \sin k_x d \sin k_y d$, with $d=a/\sqrt{2}$. In this case, an incident particle with any nonzero k_y experiences a sign change in the order parameter as it reflects from the surface.

Calculation of the bare Green's function $\hat{G}^{(0)}(n,k_y,\omega)$ from Eq. (12) gives at $\mu=0$, $G_{1,3}(n,k_y,\omega)=0$ for even n and $G_0(n,k_y,\omega)=0$ for odd n. Explicitly,

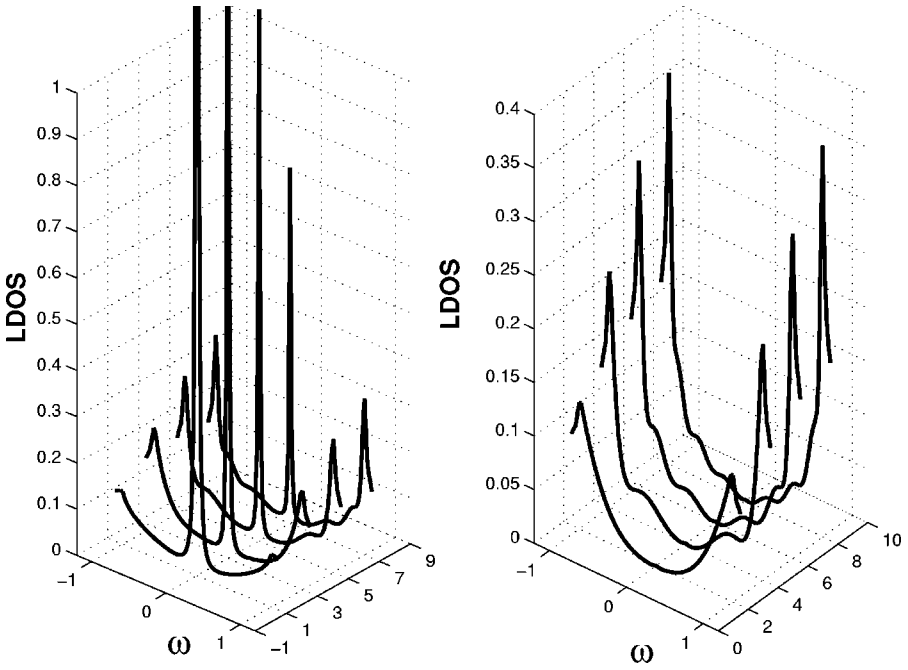

FIG. 3. Local density of states $\rho(x,\omega)$ in superconducting state vs $\omega/\Delta_{\max}$ for the case of one (110) surface, $\Delta_0=0.2t, \mu=0$. Left: chains an odd distance $n=x/d$ from surface at $x=0$. Right: chains an even distance from $x=0$.

$$\hat{G}^{(0)}(n=2m,k_y,\omega) = -\frac{i|\omega|\exp\{-i|n|z\,\mathrm{sgn}[\omega(q^2-\Delta^2)]\}}{\sqrt{(\omega^2-\Delta^2)(q^2-\omega^2)}}\hat{\tau}_0 \tag{16}$$

and

$$\hat{G}^{(0)}(n=2m+1,k_y,\omega) = \frac{i\Delta\exp\{-i|n|z\,\mathrm{sgn}[\omega(q^2-\Delta^2)]\}\mathrm{sgn}[n(q^2-\Delta^2)]}{\sqrt{(q^2-\Delta^2)(\omega^2-\Delta^2)}}\hat{\tau}_1 + \frac{iq\exp\{-i|n|z\,\mathrm{sgn}[\omega(q^2-\Delta^2)]\}\mathrm{sgn}(\omega)}{\sqrt{(q^2-\Delta^2)(q^2-\omega^2)}}\hat{\tau}_3, \tag{17}$$

where

$$z(k_y) = \tan^{-1}\sqrt{\frac{q^2-\omega^2}{\omega^2-\Delta^2}}, \tag{18}$$

$$\Delta(k_y) = 2\Delta_0\sin(k_y d), \tag{19}$$

$$q(k_y) = 4t\cos(k_y d), \tag{20}$$

and $\Delta(k_y)$ and $q(k_y)$ are the maximum gap $\Delta_{\mathbf{k}}$ and single-particle spectrum $\xi_{\mathbf{k}}$ for fixed k_y in (110) geometry. Note that here the square-root function takes positive values for positive arguments, i.e., under the conditions $|\Delta(k_y)|<|\omega|<|q(k_y)|$ or $|q(k_y)|<|\omega|<|\Delta(k_y)|$. For $A^2-\omega^2<0$, the branch $\sqrt{A^2-\omega^2}\to -i\,\mathrm{sgn}(\omega)\sqrt{\omega^2-A^2}$, for either $A=\Delta, q$. In Fig. 3 we show the LDOS spectra on the different layers. Each layer is defined as an array of sites parallel to the surface. Its index indicates its position; layer n corresponds to sites at a distance nd away from the surface.

The Andreev bound states are manifested as zero-energy peaks in the LDOS. For $\mu=0$, such states are found in all odd layers, and are absent on even ones, as seen in Fig. 4. This even-odd effect can be easily understood from the form of the T matrix and Green's functions, Eqs. (13)–(17). For even n, the bare Green's function $G^{(0)}(n,k_y,\omega)$ is proportional to ω for low frequencies. Then the T-matrix $T\sim 1/\omega$ for small ω. Even though the T matrix has a pole at $\omega=0$, the product of two Green's functions in the analog of Eq. (3) decreases faster, resulting in zero LDOS at zero frequency. As seen from the right panel of Fig. 3, the low-energy density of states on even layers near the (110) surface is substantially less than in the bulk, where it varies linearly with sufficiently low energy. Furthermore, the amplitude of the gap features in the LDOS is noticeably suppressed with decreasing distance from the surface. These features of the LDOS can be understood based on a simple relation between the Green's function $\hat{G}(n'=n,k_y,\omega)$ of the half space and the

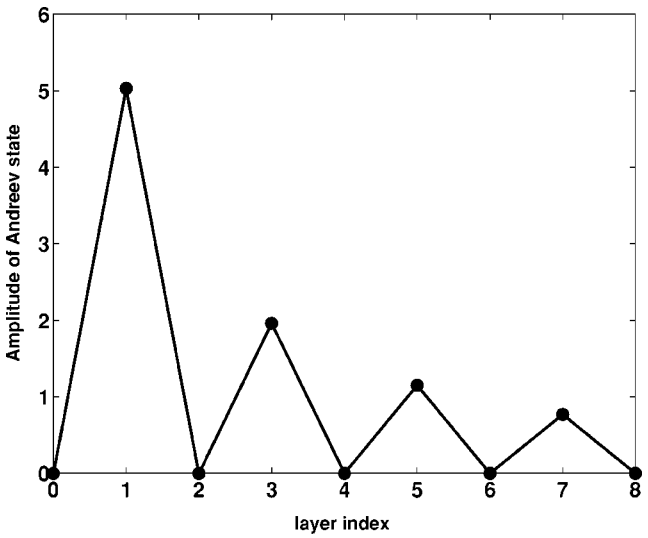

FIG. 4. Amplitude of Andreev state vs distance $n=x/d$ from (110) surface for $\Delta_0=0.2t, \mu=0$.

bare Green's function $\hat{G}^{(0)}(n-n=0,k_y,\omega)$, which takes place for even $n=2m$:

$$\hat{G}(n'=n,k_y,\omega)=\{1-\exp[-2i|n|z\ \mathrm{sgn}(\omega(q^2-\Delta^2))]\}\times\hat{G}^{(0)}(0,k_y,\omega). \quad (21)$$

The factor in the braces in Eq. (21) controls the deviation from the bulk behavior and diminishes with decreasing even $|n|$. At low energies only narrow regions of k_y near the center and the edge of the Brillouin zone contribute to the LDOS. As a result, for even layers the density of states goes as $|\omega|^3$ at low energies, with the main contributions arising from k_y near the edge of the Brillouin zone.

For odd layers, the τ_1 and τ_3 components of $\hat{G}^{(0)}(n=2m+1,k_y,\omega)$ are the ones that are nonzero, and they approach a constant value as ω goes to zero. So the pole in the T matrix generates the peak in the LDOS, associated with the zero-energy Andreev surface states. For Andreev states, z is an imaginary quantity. The size of the peak decreases as the distance to the surface increases due to the $e^{-|n\ \mathrm{Im}\ z|}$ factor in Eq. (17). For large $|n|$, small k_y dominates the integration over k_y in the LDOS and we obtain the following zero-energy asymptotic behavior of the LDOS: $\rho(\omega)=(2t/\pi\Delta_0 n^2)\delta(\omega)$. The size of the zero-energy peak in the LDOS $\propto n^{-2}$.

C. (210) surface

It is useful to study a case intermediate between the standard (100) and (110) surfaces to see what qualitatively new features arise. From the usual quasiclassical viewpoint, the weight of the zero-energy Andreev (210) surface states should be finite, but smaller than for the (110) surface because the phase space for which the reflecting quasiparticle experiences a sign change of the order parameter is reduced. The tight-binding model leads to a more complicated dependence of the weight of the zero-energy states on the surface orientations relative to the crystal axes. Thus, for the (210) surface the model shows at half filling no zero-energy Andreev states at all. We associate this discrepancy, in particular, with the difference between reflection channels incorporated in the two approaches.

Standard quasiclassical considerations imply that parallel to a smooth surface the momentum component k_y is conserved in a reflection event, and only conventional specular reflection takes place. A tight-binding model shows that, generally speaking, this is not the case, since the *crystal momentum* component k_y can also change in a reflection process by a reciprocal crystal vector along the surface. Due to a difference between reciprocal crystal vectors at the surface and in the bulk, the momentum acquired by a quasiparticle in a reflection event can be physically distinguished in the bulk from that of specularly reflecting quasiparticle. Hence, specific crystal periodicity along a particularly oriented surface can result in additional channels for quasiparticle reflection, if there is a reflected state $k_x(k_y),k_y$ on the Fermi surface corresponding to the k_y surface Umklapp process.[56]

In this case the Fermi surface, considered as a part of the surface-adapted Brillouin zone, should exhibit multiple values of outgoing $k_{F,x}$ for a fixed value of $k_{F,y}$. This situation is realized for the comparatively complicated multisheet structure of the Fermi surface in the surface-adapted Brillouin zone for the (210) surface, as obtained in Fig. 9 of Ref. 36. A strong dependence of the particular shape of the surface-adapted Brillouin zone, as well as the Fermi surface in the zone, on surface orientation is an important characteristic feature of the tight-binding models.[36,51] Within the quasiclassical theory, the shape of the Fermi surface is usually considered as independent of surface orientations relative to the crystal axes. We note that the zero-energy surface states can disappear, if multiple channels for reflection of quasiparticles from an impenetrable surface are assumed. In this section, we now study the LDOS for quasiparticle spectra obtained with the tight-binding model at half filling for (210) surface.

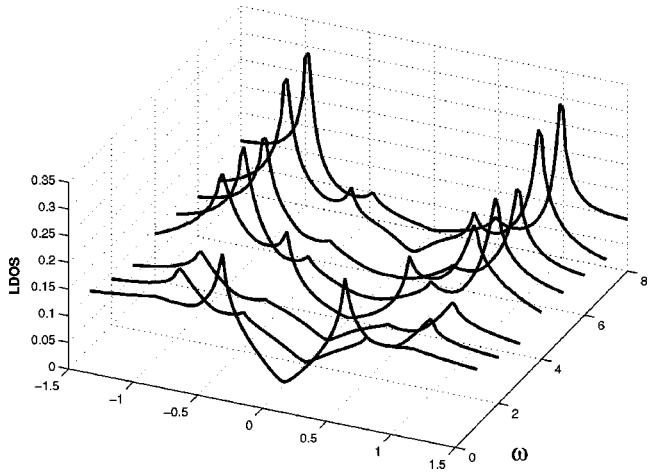

FIG. 5. Local density of states $\rho(x,\omega)$ vs $\omega/\Delta_{\max}$ for a closed (210) nontransparent surface at half filling model and $\Delta_0=0.2t,\mu=0$. Each curve corresponds to a chain located at a distance x/d to the surface.

Technically, we now need to solve for the Green's function in the presence of two impurity lines (Fig. 1). In the general case of two parallel impurity lines, we cut the crystal at an orientation given by $(hl0)$ and introduce an impurity potential

$$U(\mathbf{r})=U_0\sum_j \delta(\mathbf{r}-\mathbf{R}_j), \quad (22)$$

where $\mathbf{R}_j$ are the points on the two impurity lines, at the location of the boundaries. The first boundary is defined to be located at $x=0$ with impurity sites $\mathbf{R}_j=jd^{-1}\hat{y}$ and the other is parallel and located at $x=(N+1)d$ with $\mathbf{R}_j=(N+1)d\hat{x}+(c+jd^{-1})\hat{y}$, giving a total of N free chains. Here c is a shift along y axis of sites on the $(N+1)$th chain relative to the sites on the 0th chain. For the special case of the (210) surface, we need two adjacent lines at $x=0$ and $x=-d$, so formally this corresponds to the case of $N=-2$.

The equation for the T matrix [Eq. (4)] for this impurity potential can be solved by choosing the ansatz

$$\hat{T}(k_x,k_x',k_y)=\hat{t}_0+\hat{t}_1e^{i(N+1)dk_x}+\hat{t}_2e^{-i(N+1)dk_x'}+\hat{t}_3e^{i(N+1)d(k_x-k_x')}. \quad (23)$$

In the limit of infinitely strong impurity potential this gives

$$\hat{t}_0 = \frac{-\hat{G}^{(0)}(0)^{-1}}{1-\hat{G}^{(0)}(0)^{-1}\hat{G}^{(0)}(-N-1)\hat{G}^{(0)}(0)^{-1}\hat{G}^{(0)}(N+1)},$$

$$\hat{t}_1 = \frac{\hat{G}^{(0)}(0)^{-1}\hat{G}^{(0)}(N+1)\hat{G}^{(0)}(0)^{-1}}{1-\hat{G}^{(0)}(0)^{-1}\hat{G}^{(0)}(-N-1)\hat{G}^{(0)}(0)^{-1}\hat{G}^{(0)}(N+1)},$$

$$\hat{t}_3 = -\frac{\hat{G}^{(0)}(0)^{-1}}{1-\hat{G}^{(0)}(0)^{-1}\hat{G}^{(0)}(N+1)\hat{G}^{(0)}(0)^{-1}\hat{G}^{(0)}(-N-1)},$$

$$\hat{t}_2 = \frac{\hat{G}^{(0)}(0)^{-1}\hat{G}^{(0)}(-N-1)\hat{G}^{(0)}(0)^{-1}}{1-\hat{G}^{(0)}(0)^{-1}\hat{G}^{(0)}(-N-1)\hat{G}^{(0)}(0)^{-1}\hat{G}^{(0)}(N+1)}.$$

The Green's function in this case can then be written as

$$\hat{G}(n,n') = \hat{G}^{(0)}(n-n') - [\hat{G}^{(0)}(n)\ \hat{G}^{(0)}(n-N-1)] \times \begin{pmatrix} \hat{G}^{(0)}(0) & \hat{G}^{(0)}(-N-1) \\ \hat{G}^{(0)}(N+1) & \hat{G}^{(0)}(0) \end{pmatrix}^{-1} \begin{pmatrix} \hat{G}^{(0)}(-n') \\ \hat{G}^{(0)}(N+1-n') \end{pmatrix}, \tag{24}$$

where we have not written the dependence on k_y and ω explicitly.

The equation for the bound state on (210) surface is

$$\det \begin{pmatrix} \hat{G}^{(0)}(0) & \hat{G}^{(0)}(1) \\ \hat{G}^{(0)}(-1) & \hat{G}^{(0)}(0) \end{pmatrix} = 0. \tag{25}$$

Figure 5 displays the LDOS spectra calculated on several layers for (210) surface. There is no zero-energy peak observed on any chain at all, for the reasons explained in the beginning of this section. The peaks in the LDOS, seen close to the (210) surface at energies $\pm 0.5\Delta_{\max}$, originate from the gap features taken for the momentum along the surface normal: $\Delta(k_{F,x}, k_{F,y}=0)=0.5\Delta_{\max}$. The peak at $\omega=\Delta(k_{F,x},0)$ arises for the homogeneous model of the order parameter, while for the self-consistent spatially dependent order parameter it lies slightly below $\Delta(k_{F,x},0)$. It is associated with the surface Andreev states and decays in the depth of the superconductor. These peaks have been theoretically found first in Ref. 23 with a continuous model and then also for the conductance with a lattice model.[36] We notice that the conductance spectrum shown in Fig. 14 of Ref. 36 is in agreement with the LDOS on the first chain (at $x=d$) in Fig. 5. The variations of the LDOS from chain to chain, which accompany a large-scale behavior, are the Friedel-like oscillations.

IV. HALF-FILLED WIRES

We now consider wires where the second line of impurities confines the system to a finite width, i.e., we restrict ourselves to the cases with surface normal along the (100) and (110) directions. Semiclassically, a quasiparticle will go through multiple scatterings, bouncing back and forth between the two walls. Hence we expect that the interplay between Andreev reflection, taking place due to sign change of the order parameter, and the energy discretization, due to finite wire width, to yield novel features. We again model the surfaces by introducing impurities on the appropriate sites to completely isolate the wires. The corresponding Green's function is given by Eqs. (24). The bound-state energies are determined by the equation

$$\det \begin{pmatrix} \hat{G}^{(0)}(0) & \hat{G}^{(0)}(-N-1) \\ \hat{G}^{(0)}(N+1) & \hat{G}^{(0)}(0) \end{pmatrix} = 0. \tag{26}$$

A. (100) wires

Ziegler *et al.*[13] investigated the problem of (100) *d*-wave quantum wires in some detail, and discovered the existence of a number-parity effect as a function of the width N of a mesoscopic *d*-wave wire: a finite total DOS is found at the Fermi level for odd N and zero DOS (with a full gap in the excitation spectrum, not a *d*-wave-like gap) is found for even N, at least for a simple tight-binding band at half filling. The differences between even and odd N were shown to survive for more general bands, as well. For completeness, we reproduce, using our approach, some of their LDOS spectra in Fig. 6.

B. (110) wires

1. Normal metal wires

Based on intuition from the surface case, we would expect that Andreev states play an important role in (110) wires, with geometry shown in Fig. 7. A crucial question which arises in the following discussion is, how does one identify a subgap state of true Andreev character? By merely measuring the LDOS with an STM, for example, one may see several peak structures, not all of which will be related to Andreev reflections at the surfaces. One set of candidate states which needs to be investigated first is the set of discrete dispersive (with respect to k_y) levels which arise simply because of the finite wire width. These are of course present already in the normal-state wire.

The k_x-integrated bare normal-state Green's function for an infinite lattice above T_c takes the form

$$G_{11}^{(0)}(n,k_y,\omega) = \frac{d}{2\pi}\int_{-\pi/d}^{\pi/d} \frac{e^{ik_x nd}dk_x}{(\omega+i0)-\xi_{\mathbf{k}}} = -\frac{i\,\exp[i|n|\arccos[-\omega/q(k_y)]]}{\sqrt{q^2(k_y)-\omega^2}}, \tag{27}$$

where $q(k_y)$ is defined in Eq. (20). The full Green's function

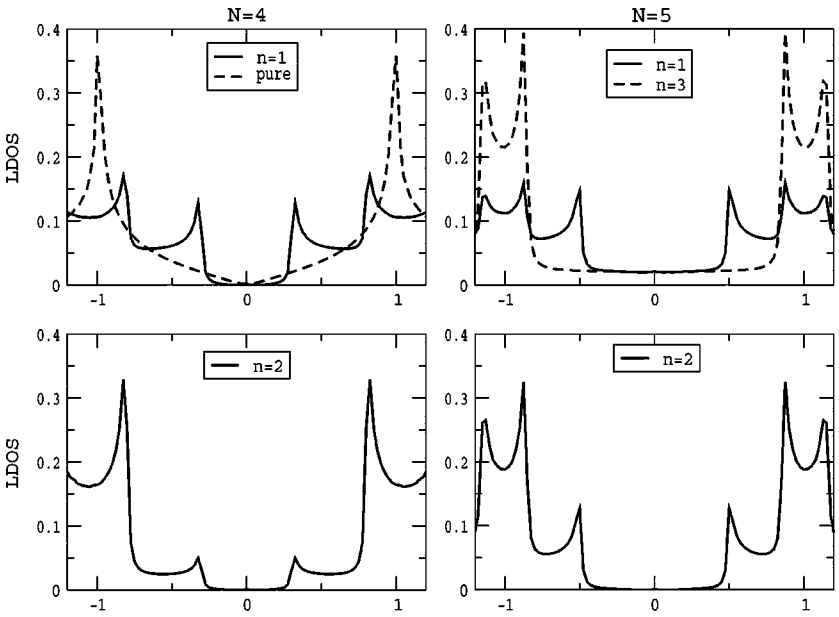

FIG. 6. Local density of states $\rho(x,\omega)$ vs $\omega/\Delta_{\max}$ for a (100) wire of width $N=4$ (left panels) and $N=5$ (right panels), using $\Delta_0=0.2t, \mu=0$.

for a (110) wire may then be obtained by solving the T-matrix equation as

$$G_{11}(n,n';k_y,\omega)=\frac{2\sin[n_{\min}z]\sin[(n_{\max}-N-1)z]}{\sqrt{q^2(k_y)-\omega^2}\sin[(N+1)z]}, \tag{28}$$

where $n,n'=1,2,\ldots,N, z\equiv z(k_y,\omega)=\cos^{-1}[-\omega/q(k_y)], n_{\min}=\min(n,n')$, and $n_{\max}=\max(n,n')$.

For every value of k_y, there generally exists a series of eigenvalues which are the poles of the Green's function. They may be obtained by simply solving

$$\sin[(N+1)z(k_y,\omega)]=0, \tag{29}$$

which yields

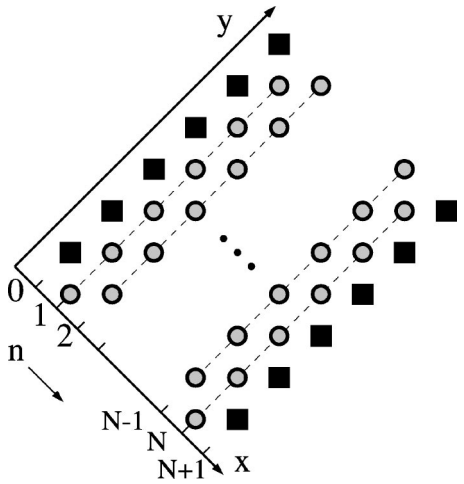

FIG. 7. Geometry of (110) wire (sites are filled circles) of width N bounded by two impurity lines (filled squares). Wire is infinite in both y and $-y$ directions.

$$\omega_\nu(k_y)=-q(k_y)\cos\frac{\pi\nu}{N+1}, \quad \nu=0,1,\ldots,N+1. \tag{30}$$

This gives N branches of solutions for $\nu=1,\ldots,N$, distributed symmetrically with respect to the Fermi level, and two special solutions ($\nu=0$ and $N+1$) with $\omega=\pm q(k_y)$ which we refer to as defining the "effective band edge". One interesting feature is the existence in the normal metal wire of dispersionless zero-energy quasiparticle states (ZES) which form the branch $\nu=(N+1)/2$ when the width N of the wire is odd. Since the group velocity vanishes for dispersionless states, they are always localized. We note that the case $N=1$ has only the obvious dispersionless ZES since no transport is allowed with only nearest-neighbor hopping. In the general $N=$odd case, it appears that there is always exactly one such localized state (doubly degenerate in particle-hole space) for any fixed k_y. A deviation from half filling shifts the zero-energy states to $-\mu$. Thus, for positive μ they are the hole states, while for $\mu<0$ they are the electron states.

The contribution of each of these states to the LDOS can be estimated by examining the residue near the pole, where the Green's function can be approximated as

$$G(n,n';k_y,\omega)\approx\frac{Q_\nu(n,n')}{\omega-\omega_\nu(k_y)}, \tag{31}$$

with the residue given by

$$Q_\nu(n,n')=\frac{2\sin\frac{n\pi\nu}{N+1}\sin\frac{n'\pi\nu}{N+1}}{N+1}, \tag{32}$$

where n is the index of the layers. Note from Eq. (32) and the spectral representation of the Green's function near a pole that it is easy to read off the quasiparticle wave functions as $\psi_\nu(n)=\sqrt{2/(N+1)}\sin[n\pi\nu/(N+1)]$, i.e., just the wave functions of a free particle confined to a box of width $(N+1)d$.

It is easy to check that for any n,n' the residue Q_ν vanishes everywhere for the "states" at the effective bandwidth

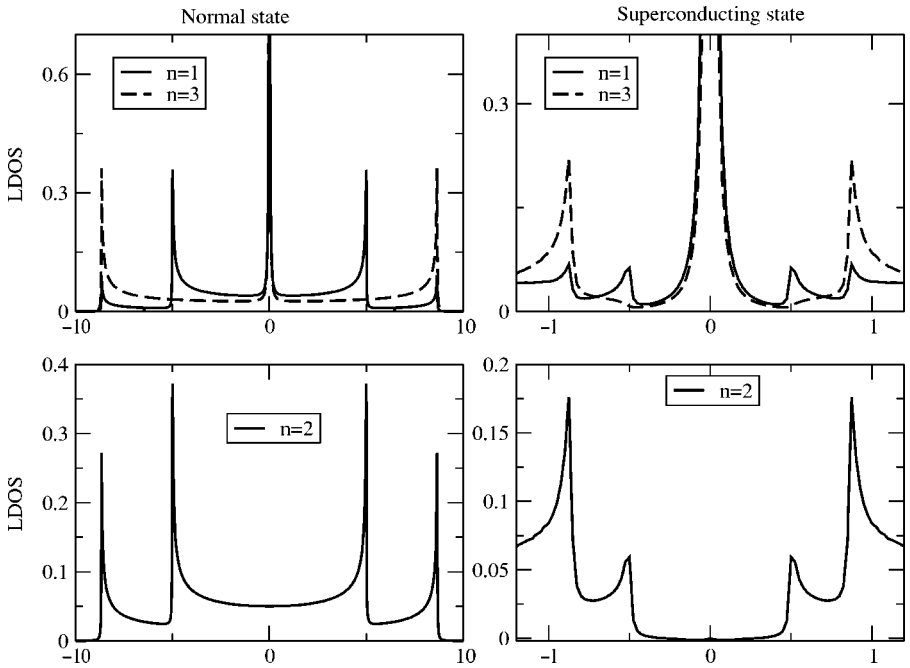

FIG. 8. Local density of states for a (110) wire of width $N=5$, with $\Delta_0=0.2t, \mu=0$. Left: normal state, $\rho(x,\omega)$ vs $\omega/\Delta_{\max}$; right: superconducting state, $\rho(x,\omega)$ vs $\omega/\Delta_{\max}$.

$\nu=0$ or $N+1$; we therefore do not discuss them further, but focus on the N branches with finite residue. For these states the residue can vanish locally on chains with number n, for which the quantity $n\nu/(N+1)$ is an integer. The odd-N ZES, for example, has a residue

$$Q_{[(N+1)/2]}(n,n) = \frac{2\left(\sin\frac{n\pi}{2}\right)^2}{N+1}. \tag{33}$$

As is seen from Eq. (33), the probability density of the ZES oscillates with a period $2d$, taking finite values only for odd n and vanishing on all nearest-neighbor sites (where n is even). This is also valid for the states with energies $\pm\mu$ in the case of the deviation from half filling and ensures no transport with nearest-neighbor hopping for quasiparticles with energies $\pm\mu$.

All these states are not surface-bound states, as one can easily check that their amplitude does not decay across the wire. The quasiparticle spectrum is discrete (for fixed k_y) due to the finite width of the wire and transforms into conventional continuous quasiparticle spectrum in the massive normal metal in the limit $N\to\infty$. The momentum resolved LDOS in the normal metal wire with discrete dispersive states takes the form

$$\rho(n,k_y,\omega) = \sum_{\nu=1}^{N} Q_\nu(n=n')\,\delta[\omega-\omega_\nu(k_y)]. \tag{34}$$

The integration over k_y gives the LDOS,

$$\rho(n,\omega) = \frac{1}{2\pi d}\sum_{\omega_\nu(k_y)=\omega}\frac{Q_\nu(n,n)}{|d\omega_\nu/dk_y|}, \tag{35}$$

where the sum is taken over those k_y and ν, which satisfy the equation $\omega_\nu(k_y)=\omega$.

The position of peaks in LDOS are then determined by extrema of the dispersive branches, Eq. (30), taking place at $k_y=0$:

$$\omega_{\nu,\text{peaks}} = -4t\cos\frac{\pi\nu}{N+1}, \quad \nu=1,\ldots,N. \tag{36}$$

The peaks corresponding to the N normal metal wire states are seen clearly in Figs. 8 and 9 at the eigenfrequencies given by Eq. (36). It is easy to check that the weights agree with Eq. (32). The LDOS for the normal metal wires qualitatively differs from the LDOS for bulk normal metals with the nearest-neighbor hopping on the square lattice. The zero-energy peak (the Van Hove singularity) in the bulk metal is symmetric as a function of the energy and its log singularity is much broader than the δ-like peaks we find here for wires.

2. Superconducting wires

The T matrix and Green's-function equations are necessarily more complicated in the presence of superconductivity, but they are still tractable in the (110) case. The bare Green's functions $\hat{G}^{(0)}$ are given by Eqs. (16) and (17), as before. One must then solve Eq. (26), which applies to any situation which requires two lines of impurities, for the eigenenergies ω. Similar to the normal metal case, there are special solutions of Eq. (26): $\omega=\pm\Delta(k_y), \omega=\pm q(k_y)$ for any N and $\omega=0$ for even N. They are poles of the T matrix, but do not correspond to the poles of the full Green's function.

The behavior of subgap surface states on the narrow superconducting wire differs qualitatively from the case of the superconducting half space due to the interference of the wave functions of the states on both surfaces. Since the zero-energy peak in the LDOS for the half-filled surface vanishes on each even chain (see Figs. 3 and 4), the spectrum of Andreev states on the (110) wires becomes strongly dependent on the parity of the number N of chains in the half-filled

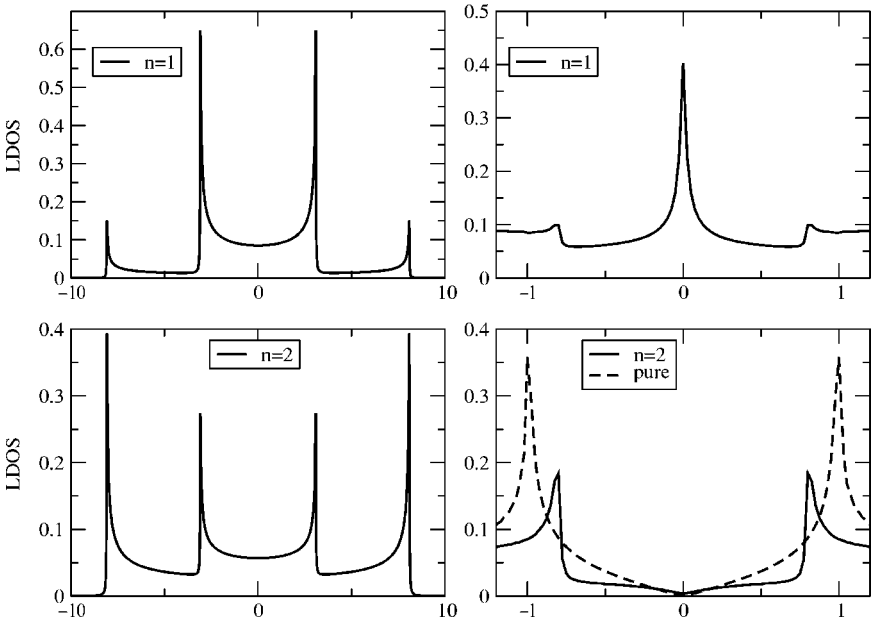

FIG. 9. LDOS for a (110) wire of width $N=4$ with $\Delta_0=0.2t, \mu=0$. Left: normal state, $\rho(x,\omega)$ vs $\omega/\Delta_{\max}$; right: superconducting state, $\rho(x,\omega)$ vs $\omega/\Delta_{\max}$.

wire. This effect is quite pronounced for wires whose width is the order of or less than the superconducting coherence length. As we demonstrate below, some new qualitative features arising in the superconducting state of the (110) wires in the quasiparticle spectrum above $\Delta(k_y)$ [see Eq. (19)] can also be strongly dependent on the parity of N.

Odd N. For a wire with odd N, only the Green's functions (16) with even arguments $n=0,\pm(N+1)$ enter Eq. (26). Since at small frequencies these Green's functions are $\propto\omega$, it is straightforward to show that the only subgap state is a dispersionless ZES $\omega=0$. Dispersive modes exist as well and take the form

$$\omega_\nu^2(k_y)=q^2(k_y)\cos^2\frac{\pi\nu}{N+1}+\Delta^2(k_y)\sin^2\frac{\pi\nu}{N+1},$$

$$\nu=1,\ldots,\frac{N-1}{2}. \tag{37}$$

This exactly coincides with the quasiparticle spectrum in a bulk two-dimensional superconductor, $\omega^2(k_y,k_x)=\xi^2(k_y,k_x)+\Delta^2(k_y,k_x)$, if the discrete values of momentum component across the wire, $k_{x,\nu}=\pi\nu/(N+1)d$, are introduced. We note that the dispersionless zero-energy Andreev states are the only true subgap states in the spectrum, since the energy $|\omega_\nu(k_y)|$ of the dispersive states (37) lies above the respective value $|\Delta(k_y,k_x)|$ of the order parameter, for any ν and k_y.

There are, as in the normal state case, $N-1$ dispersive modes in addition to the ZES. They are doubly degenerate due to the particle-hole symmetry. This simple result can be understood as follows. For a fixed k_y the problem reduces to a one-dimensional problem. The corresponding two-component Bogoliubov–de Gennes wave function takes its values on N sites, resulting in $2N$ degrees of freedom in the system. With this point of view it appears natural that for fixed k_y the total number of levels, which are twice degenerate, is N. The set of levels with positive energies for $N=11$ is represented in panel (a) of Fig. 10.

The LDOS for the superconducting wires with $N=5$ is shown in the right panel of Fig. 8. The dispersionless ZES results in a pronounced peak at zero energy on odd layers. Furthermore, each extremum of the dispersive mode $\omega(k_y)$ results in the peak in the LDOS at the energy $\omega_{k_{y,\mathrm{extr}}}$. One series of peaks is associated with the extrema at $k_y=0$. Since $\Delta(k_y=0)=0$, the peaks lie at the same positions as in the normal metal wire (36). Although they are irrelevant to the superconducting properties of the wire, some of these peaks can lie at finite energies below the maximum of the gap function, $\Delta_{\max}=2\Delta_0$. For instance, the lowest position at finite energies of the peaks of this series is $4t\sin[\pi/(N+1)]$. This can be both above or below $\Delta_{\max}$, depending on the ratio $\Delta_{\max}/t$ and the wire width N. In contrast with the normal metal wires, the dispersive quasiparticle modes [Eq. (37)] in the superconducting wires have extrema also at the edge of the surface-adapted Brillouin zone $k_y=\pm\pi/(2d)$.[57] They are shown in panel (b) of Fig. 10 for the wire with $N=11$. This leads to additional series of $(N-1)$ quasiparticle peaks in the LDOS for the superconducting wires, which lie below $\Delta_{\max}$:

$$\omega_{\mathrm{peaks}}=\pm\Delta_{\max}\sin\frac{\pi\nu}{N+1},\quad \nu=1,\ldots,\frac{N-1}{2}. \tag{38}$$

Panel (c) of Fig. 10 displays the series of peaks in the LDOS for $N=11$.

The dispersive states forming the nonzero low-energy peaks (38) in LDOS are *not* Andreev states. They lie below $\Delta(k_y)$ for k_y near the edges of Brillouin zone, but they are situated above the bulk gap function $\Delta[k_x(\nu),k_y]$. The wave function for any of these states possesses the finite current of the probability density, while for Andreev states the total probability current vanishes.

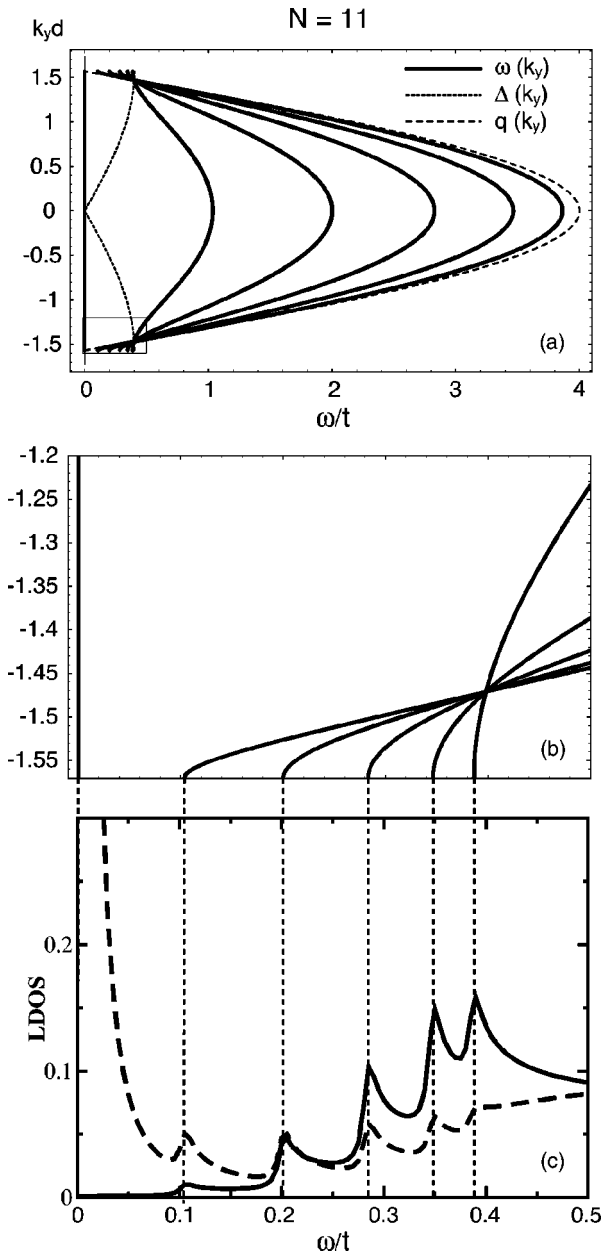

FIG. 10. Quasiparticle spectra and the LDOS for superconducting half-filled (110) wire with $N=11$. (a) Dispersive modes ($k_y d$ vs ω/t) for $N=11, \Delta_0=0.2t$, and $\mu=0$. (b) The blowup of the dispersive spectra near the edge of the Brillouin zone. (c) The LDOS for energies less than $\Delta_{\max}$: $n=2$ (solid line) and $n=1$ (dashed line), where a broadening $\delta=0.005t$ has been used.

While positions of the peaks are determined by the extrema of the dispersive energies, their weights in the LDOS are controlled also by quasiparticle wave functions, which form the quantity $Q(n,n)$ in Eq. (35). For this reason the weights of the peaks can substantially differ on different layers and may vanish on some of them, quite analogous to the normal metal wires [see Eq. (32)]. Due to an interference from two surfaces, the wave function, taken on even layers, turns out to coincide with the respective wave function in the normal metal case (apart from a normalization constant). On the other hand, the wave function on odd layers is a superposition of electronlike and holelike Bogoliubov quasiparticles on the wire.

Even N. In the case of even-N half-filled wires, the quasiparticle spectra become more complicated. The Green's functions (16) and (17) with even ($n=0$) and odd [$n=\pm(N+1)$] arguments enter Eq. (26), which can be reduced to the following form:

$$q(k_y)\tan[(N+1)z] = \alpha\Delta(k_y)\tan z, \tag{39}$$

where $\alpha=\pm 1, 0\leqslant z\leqslant \pi/2$. Solutions $z_{\nu,\alpha}(k_y)$ of Eq. (39) are directly associated with ω, in accordance with Eq. (18):

$$\omega^2_{\nu,\alpha}(k_y) = q^2(k_y)\cos^2 z_{\nu,\alpha}(k_y) + \Delta^2(k_y)\sin^2 z_{\nu,\alpha}(k_y). \tag{40}$$

Here $\nu=1,\ldots,(N/2)$ and α are the indices of the solution. Comparing Eqs. (37) and (40) for the spectra of odd and even wires, one can see that z/d plays the role of effective discrete values of the momentum component k_x (at fixed k_y) across the wire. Equation (39) can be transformed to a polynomial equation in $\tan z$ of the Nth degree, if one excludes the special solutions $\omega=\pm\Delta(k_y), \pm q(k_y)$ mentioned above. Hence, for a fixed α there are exactly $N/2$ positive and $N/2$ negative solutions for ω, describing N dispersive branches of the quasiparticle spectrum. Explicit analytical form of the spectra can be easily found from Eqs. (39) and (40) in the particular cases $N=2$,

$$\omega_\alpha = \pm\frac{1}{2}[q(k_y) + \alpha\Delta(k_y)], \tag{41}$$

and $N=4$ ($\nu=\pm, \alpha=\pm$),

$$\omega^2_{\nu,\alpha}(k_y) = \Delta^2(k_y) + \frac{1}{8}q(k_y)[q(k_y)+\alpha\Delta(k_y)]\left[3 - 5\alpha\frac{\Delta(k_y)}{q(k_y)} + \nu\sqrt{5 - 6\alpha\frac{\Delta(k_y)}{q(k_y)} + 5\frac{\Delta^2(k_y)}{q^2(k_y)}}\right]. \tag{42}$$

Equation (42) is defined for all k_y in the Brillouin zone for which $\omega^2_{\nu,\alpha}(k_y)$ is positive. Equations (41) and (42) describe the quasiparticle spectra for non-self-consistent wires with small numbers of chains. As we will show in Sec. V, the self-consistent treatment of the problem can lead to important modifications of the results, at least if the width of the wire is less than or of order the superconducting coherence length.

Whereas in the normal metal state, ν is the only index of the solution (for a given k_y), in the superconducting even-N wire each branch with fixed ν splits into two, corresponding to two values of the index α, giving a total of $2N$ distinct branches. Since the order parameter vanishes for $k_y=0$, the splitting is absent in this particular case. The splitting is associated with the symmetry breaking of the eigenstates with respect to the sign reversal of k_y. In the normal even-N wires, as well as in the odd-N wires (both in the normal metal and in the superconducting states), each separate branch of the spectra $\omega_\nu(k_y)$ is an even function of k_y. This is not the case, however, for the even-N superconducting (110) wires. As directly seen from Eq. (39) and the relations $q(-k_y)=q(k_y), \Delta(-k_y)=-\Delta(k_y)$, the solutions of Eq. (39), $z_{\nu,\alpha}(k_y)$, with fixed α are not odd or even functions of k_y, due to the

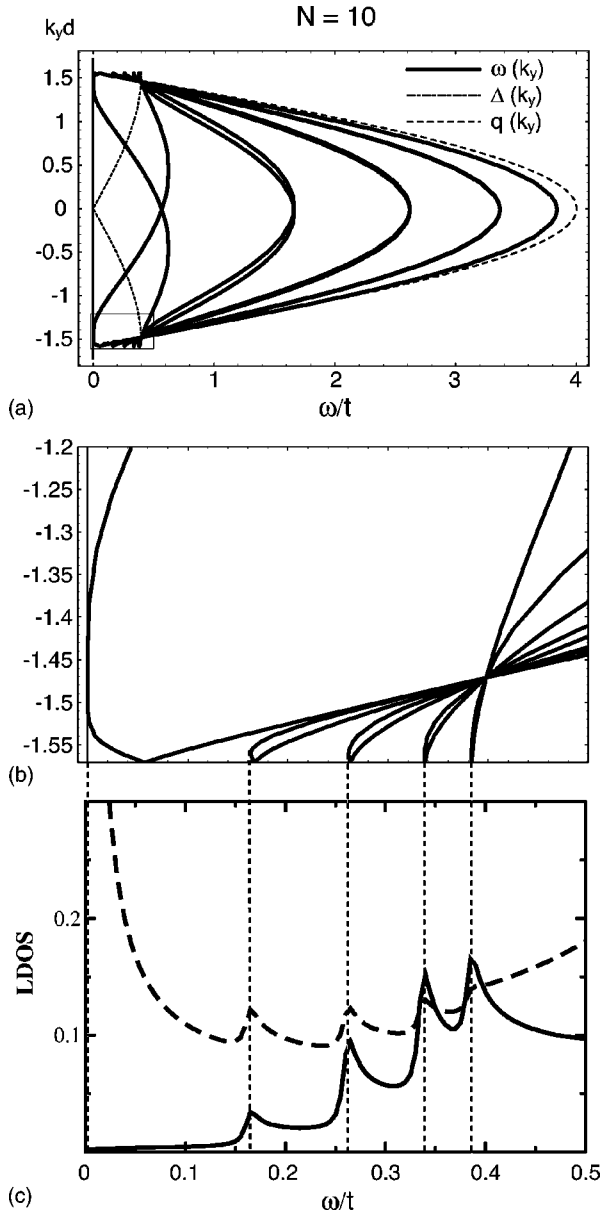

FIG. 11. Quasiparticle spectra and the LDOS for superconducting half-filled (110) wire with $N=10$. (a) Dispersive modes ($k_y d$ vs ω/t) for $N=10, \Delta_0=0.2t, \mu=0$. (b) The blowup of the spectra near the edge of the Brillouin zone. (c) The LDOS for energies less than or equal to $\Delta_{\max}$: $n=2$ (solid line), $n=1$ (dashed line), where a broadening $\delta=0.005t$ has been used.

nonzero right-hand side of Eq. (39) in the superconducting state. Evidently, each separate branch of the spectra $\omega_{\nu,\alpha}(k_y)$ possesses the same property. The whole spectrum, however, remains symmetric with respect to $k_y \to -k_y$, since the branches with positive and negative α simply interchange with each other under this transformation. Spectra of the half-filled $N=10$ superconducting wire with positive energies are shown in panel (a) of Fig. 11. They agree with the above discussion. For branches with higher energies, the splitting is less than for lower branches. For small splittings, $\delta\omega \propto \Delta/(N+1)$.

The splitting manifests itself by slightly shifting the positions of peaks in the LDOS, due to respective shifts of extrema of dispersive quasiparticle energies. In contrast with the double number of extrema, the total number of the peaks in the LDOS does not change. Any peak in the LDOS originates from the two extrema, situated symmetrically with respect to the sign of k_y. Each pair of extrema belongs to two spectral branches, which differ only by their index $\alpha=\pm 1$. If we disregard the splitting of the quasiparticle spectra, the positions of the peaks in the LDOS coming, for example, from the edge of the Brillouin zone, are as follows:

$$\omega_{\text{peaks}} = \pm \Delta_{\max} \cos\frac{\pi\nu}{N+1}, \quad \nu = 1, \ldots, \frac{N}{2}. \tag{43}$$

The splitting shifts the peak positions towards slightly lower energies $|\omega|$, as compared with those in Eq. (43). The respective extrema of dispersive energies are shifted towards lower values of $|k_y|$ from $k_y=\pm\pi/(2d)$. These low-energy peaks in the LDOS are shown in panel (c) of Fig. 11.

The other peaks in the LDOS come, neglecting the splitting, from the center of the Brillouin zone. Since the order parameter vanishes in the center of the zone, the positions of the peaks are still the same as in Eq. (36) for the normal metal state. The splitting, taking place in the superconducting state, slightly shifts the extrema of the spectra from the center of the zone, so that the peaks move to larger energy values $|\omega|$, as compared with those in Eq. (36).

The LDOS for the superconducting wire with $N=4$ is shown in the right panel of Fig. 9. In addition to the peaks at finite energies, discussed above, there is also a well-pronounced zero-energy peak there [see also panel (c) of Fig. 11]. This peak originates from the extrema of two dispersive branches of Andreev states, which take place at $\pm k_{y,0}d = \pm\tan^{-1}(2t/\Delta_0)$, where the relation $q(k_{y,0})=\Delta(k_{y,0})$ holds. Indeed, as follows from Eqs. (18) and (39) and, in particular, directly seen from Eq. (42), the energy and its derivative equal zero for $k_y=\pm k_{y,0}$. It turns out that the multiplicity of zeros of the lowest dispersive branches of states at the extrema $k_y=\pm k_{y,0}$ is $N/2$, i.e., $\omega \propto |k_y - k_{y,0}|^{N/2}$ in the close vicinity of $k_{y,0}$. This follows directly, for instance, from Eq. (50) given below. We notice that the lowest dispersive curve in panel (b) of Fig. 11 manifests very slow change of energy when it touches the zero-energy line. This agrees with our expectation $\omega \propto |k_y - k_{y,0}|^5$ for the (110) wire with $N=10$. The respective peak in the LDOS of wires with large even N diverges at $\omega=0$, but is not a δ-like peak as it is for wires with odd N.

The identification of the Andreev nature of the quasiparticle bound states in confined geometries turns out to be a nontrivial problem, at least in the case of half-filled (110) wires with even N, where there is a symmetry breaking with respect to $k_y \to -k_y$. As seen from Eqs. (39)–(42), the asymmetry can be associated with the order-parameter behavior $\Delta(-k_y)=-\Delta(k_y)$ and with the sensitivity of the quasiparticle energies to the π shift of the order-parameter phase. A dependence of the dispersive energy curve on the order-parameter phase is usually an intrinsic feature of Andreev bound states only. We consider the vanishing of the probability density current as an defining property of Andreev bound states. These states should be able to carry finite electric

current, however. In odd-N wires only zero-energy dispersionless quasiparticle states satisfy the above requirements. In even N (110) wires the zero-energy dispersionless states do not arise at all. The interference of wave functions located near two surfaces of the even-N wire induces dispersive Andreev branches $\pm\omega_A(k_y)$, which transform into the zero-energy states in the limit of infinitely large N. Moreover, all quasiparticle states in the half-filled (110) superconducting wire with even N, even those lying above the gap, turn out to satisfy the above-mentioned conditions, i.e., possess the properties of Andreev bound states. As an example, we describe below in detail the structure of the lowest dispersive quasiparticle branch, which we denote as Andreev branch $\omega_A(k_y)$, although its energy varies with k_y over a large range, including both the subgap and the supergap regions (see, for example, Fig. 11).

For those k_y where $\min\{|\Delta(k_y)|, q(k_y)\} < |\omega_A(k_y)| < \max\{|\Delta(k_y)|, q(k_y)\}$, the wave function of the state can be written on odd layers ($n=2m+1$) as

$$\begin{pmatrix} u \\ v \end{pmatrix} = C \,\mathrm{sgn}\,\omega_A \sin[(N+1-n)z] \begin{pmatrix} 1 \\ i\,\mathrm{sgn}\,k_y \end{pmatrix}, \tag{44}$$

and on even layers $n=2m$

$$\begin{pmatrix} u \\ v \end{pmatrix} = C(-1)^{N/2} \sin(nz) \begin{pmatrix} 1 \\ -i\,\mathrm{sgn}\,k_y \end{pmatrix}. \tag{45}$$

In the range of k_y for which $|\omega_A(k_y)| < \min\{|\Delta(k_y)|, q(k_y)\}$, the quantity z, entering Eq. (40), becomes imaginary. Under the condition $|\omega_A(k_y)| < |\Delta(k_y)| < q(k_y)$ the wave function takes the following form on odd layers ($n=2m+1$):

$$\begin{pmatrix} u \\ v \end{pmatrix} = C_1(-1)^m \mathrm{sgn}\,\omega_A \sinh[(N+1-n)z_1] \begin{pmatrix} 1 \\ i\,\mathrm{sgn}\,k_y \end{pmatrix}, \tag{46}$$

and on even layers $n=2m$

$$\begin{pmatrix} u \\ v \end{pmatrix} = C_1(-1)^m \sinh(nz_1) \begin{pmatrix} 1 \\ -i\,\mathrm{sgn}\,k_y \end{pmatrix}. \tag{47}$$

Analogously, if $|\omega_A(k_y)| < q(k_y) < |\Delta(k_y)|$, the wave function on odd layers ($n=2m+1$)

$$\begin{pmatrix} u \\ v \end{pmatrix} = C_2 \mathrm{sgn}\,\omega_A \sinh[(N+1-n)z_1] \begin{pmatrix} 1 \\ i\,\mathrm{sgn}\,k_y \end{pmatrix}, \tag{48}$$

and on even layers $n=2m$,

$$\begin{pmatrix} u \\ v \end{pmatrix} = C_2 \sinh(nz_1) \begin{pmatrix} 1 \\ -i\,\mathrm{sgn}\,k_y \end{pmatrix}. \tag{49}$$

Here C, C_1, and C_2 are normalization constants, $z_1 = |\mathrm{Im}\, z(\omega_A(k_y), k_y)|$, z is defined in Eq. (18) and taken at $\omega = \omega_A(k_y)$.

The condition $|u(n,k_y)| = |v(n,k_y)|$, which is valid for all solutions, Eqs. (44)–(49), results in zero total probability current density, while the electric current does not vanish for the given branch. This ensures the Andreev character, as defined above, of all the states in even N wires, regardless of whether their energies lie above or below the gap.

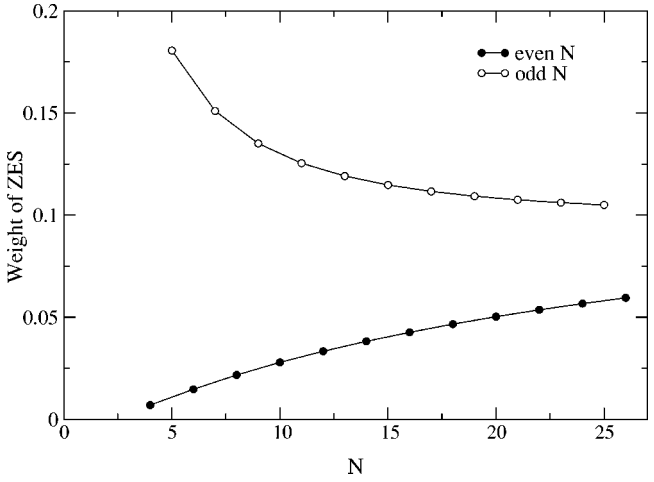

FIG. 12. The weight of the zero-energy peak in the LDOS, taken at the first layer, as a function on odd (open circles) and even (filled circles) N.

The quasiparticle states which belong to the same dispersive branch $\omega_A(k_y)$ can have their wave functions both symmetrically decaying in the depth of the wire [Eqs. (46)–(49)] or oscillating and forming standing waves across the wire [Eqs. (44) and (45)]. In particular, the amplitude of the wave functions in Eqs. (46)–(49) takes its maximum value on layers $n=1$ and $n=N$, and manifests Friedel-like oscillations, as the layer index changes from odd to a neighbor even value or vice versa. On a larger scale the amplitude decays in the bulk of the wire symmetrically with respect to two surfaces.

It is instructive to follow how the above results transform into the well-known dispersionless zero-energy Andreev surface states in the limit of large N. For sufficiently large width of the wire compared with the coherence length, and for those k_y where the wave function decays in the depth of the wire, the dispersive energy $\omega_A(k_y)$ takes a relatively simple form:

$$\omega_A(k_y) = \pm \frac{2\Delta(k_y)q(k_y)}{\sqrt{|q^2(k_y) - \Delta^2(k_y)|}} \times \exp\left[-(N+1)\sinh^{-1} \frac{\min\{|\Delta(k_y)|, q(k_y)\}}{\sqrt{|q^2(k_y) - \Delta^2(k_y)|}} \right]. \tag{50}$$

It follows from Eq. (50) that the energy of the Andreev states is exponentially small and vanishes in the limit of infinitely large N. With decreasing energy, the range of k_y where the wave function oscillates [see Eqs. (44) and (45)], converges to the center and to the edges of the Brillouin zone and finally collapses to the respective points. Hence, in the limit of very large N the amplitude of the wave function decays inside the wire for practically all values of k_y. This means that for $N \to \infty$ the dispersive branch $\omega_A(k_y)$ transforms into the zero-energy dispersionless surface states situated near the two surfaces.

Figure 12 shows N dependence of the weight of the zero-energy peak in the LDOS. For odd N, the weight diminishes with increasing N, while for even N it increases. In the limit

of large N the two curves will converge to the weight for the zero-energy surface states when the surfaces are infinitely far apart. The odd-even effects become negligibly small only for $Nd \gg \xi_0$. One could try to recover the quasiclassical results for wide wires $Nd \gg a$ after averaging over odd and even film widths. The boundary conditions for quasiclassical propagators are taken somewhere on a distance l from the surface and imply some uncertainty about the boundary positions, as well as the film (wire) thickness ($a \ll l \ll \xi_0$). As seen from Fig. 12, averaging of the weights of the peaks over odd and even N will strongly reduce their width dependence. This kind of averaging is much closer (although not identical) to the quasiclassical results on the width dependence of the LDOS for the d-wave superconducting film.[50] Very recent quasiclassical results,[58] treating various wire orientations, demonstrate the appearance of energy bands of quasiparticle states, in particular, for (110) wires. Our microscopic model for high-quality half-filled wires with fixed number of chains gives, however, only a couple of branches, Eq. (50), for even-N wires and the dispersionless zero-energy states for odd-N wires. We associate the difference between the microscopic and the quasiclassical results with the particular condition of half filling. The quasiclassical approach implies no singular behavior of the LDOS in the normal metal state near the Fermi surface, whereas the Van Hove singularity takes place in the LDOS on the Fermi surface for the normal metal state of half-filled infinite square lattice. An agreement of our microscopic results with the quasiclassical ones arises in the presence of deviations from half filling [see below Eqs. (52) and (53)].

As already mentioned, in the even-N wires the particle-hole structure of any quasiparticle states with broken $k_y \to -k_y$ symmetry satisfies the condition $|u(n,k_y)| = |v(n,k_y)|$. Our picture is that for the states above the gap this Andreev particle-hole structure is generated by the infinite sequence of "overbarrier" (overgapped) Andreev reflections, induced by a sign reversal of the order parameter, which the quasiparticles experience along their trajectories being bounded inside the wire with impenetrable surfaces. This unconventional feature does not take place for the states above the gap in the odd-N wires, since the two surfaces always result in the standing waves across the wire with no important interference effects in this case. For negligibly small splitting one should consider a superposition of two wave functions, describing the two split states. Then the Andreev structure of initially nondegenerate wave functions is lost, since the moduli of particle and hole amplitudes can easily differ from each other. The Andreev structure of quasiparticle wave functions can be lost also in the presence of deviations from the half filling, if μ is larger or of the same order as the splitting. Since the splitting vanishes for $k_y = 0$, one can expect that for sufficiently small k_y the Andreev structure of the wave functions will be destroyed even for small μ. In the following section some other consequences of deviations from half filling are considered.

3. Deviations from half filling

The shape of the Fermi surface depends on μ and has a strong influence on the low-energy quasiparticle spectrum.

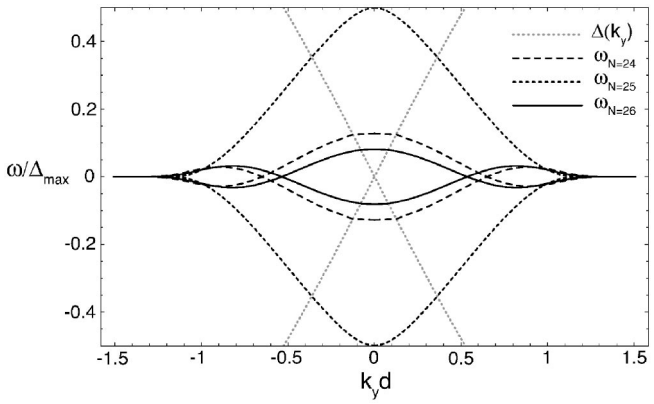

FIG. 13. The lowest energy branches for $N=24,25,26$. The parameters are $t=2.5, \mu=0.2t=0.5, \Delta_0=0.2t=0.5$, and $\Delta_{\max}=2\Delta_0=1$.

Consider, for example, low-energy quasiparticle states under the conditions $|\omega|, |\Delta(k_y)| \ll q(k_y)$. This ensures that the quasiparticle energies lie close to the Fermi surface and one can take their energies in the normal metal state to be in the linear form $\propto \mathbf{v}_F \cdot (\mathbf{k} - \mathbf{k}_F)$. Under this approximation, effects of the particle-hole asymmetry are small and one can use a quasiclassical approximation, which is valid for quasiparticles close to the Fermi surface. Then only the order parameter on the Fermi surface $\Delta(k_{F,x}, k_{F,y})$ enters the equations. For the wire geometry the momentum component $k_{F,y}$ is an independent parameter, while $k_{F,x}(k_{F,y})$, and $\Delta[k_{F,x}(k_{F,y}), k_{F,y}]$ are actually functions of $k_{F,y}$. For $\mu=0$ the Fermi surface for the (110) wire is a square with sides parallel to x or y axis. Hence, $k_{F,x} = \pm\pi/(2d)$ actually does not depend on $k_{F,y}$ in this case and $\Delta[\pm\pi/(2d), k_{F,y}] = \pm\Delta(k_{F,y})$, in accordance with Eq. (19). For finite μ we find $\Delta(k_{F,x}, k_{F,y}) = [\Delta(k_{F,y})/q(k_{F,y})]\sqrt{q^2(k_{F,y}) - \mu^2}$.

In the case of superconducting wires the equation for quasiparticle subgap energies near the Fermi surface $|\omega| < |\Delta(k_{F,x}, k_{F,y})|$ takes the form

$$\omega^2 \left(\sinh^2 \left[(N+1) d \frac{\sqrt{\Delta^2(k_{F,x}, k_{F,y}) - \omega^2}}{|v_{x,f}(k_{F,y})|} \right] + \sin^2 \phi(k_{F,y}) \right) = \Delta^2(k_{F,x}, k_{F,y}) \sin^2 \phi(k_{F,y}), \tag{51}$$

where $\phi(k_{F,y}) \equiv k_{F,x} d(N+1)$. The lowest branches of quasiparticle spectra, which follow from Eq. (51) for $N=24$, 25, 26, are shown in Fig. 13. The solution of Eq. (51) reduces to a simple form in the limit of large N:

$$\omega_A(k_{F,y}) = \pm 2\Delta(k_{F,y}) \sin \phi(k_{F,y}) \times \exp \left[-(N+1) d \frac{|\Delta(k_{F,y})|}{|v_{x,f}(k_{F,y})|} \right]. \tag{52}$$

For half-filled wires, when $\mu=0$, the phase $\phi(k_{F,y})$ does not depend on $k_{F,y}$, being equal to $\phi_{\text{odd}} = m\pi$ for odd-N wires and $\phi_{\text{even}} = (m+1/2)\pi$ for even-N wires. This difference between the phases ϕ_{odd} and ϕ_{even} plays an important role in forming well-pronounced odd-even effects in the spectra of wires with odd and even numbers of layers. Indeed, for half-filled odd-N wires Eq. (52) reduces to the zero-energy dis-

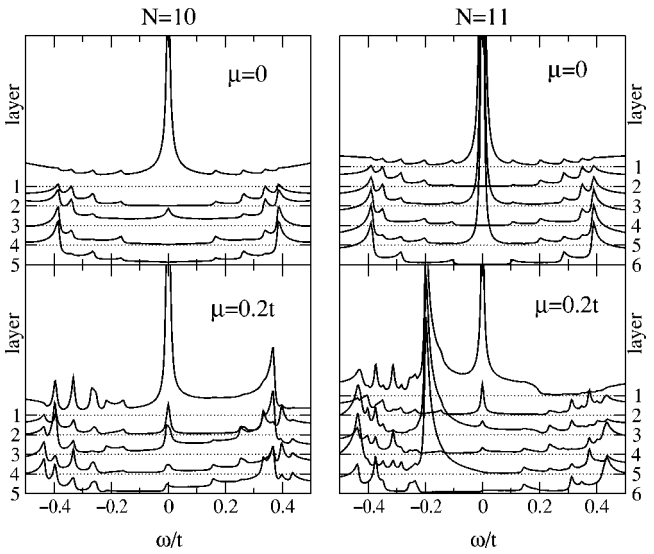

FIG. 14. Local density of states for a (110) wire with $N=10$ (left column) and $N=11$ (right column); $\mu=0$ (upper panels), $\mu=0.2t$ (lower panels). On each panel the different curves represent various chains.

persionless Andreev states. At the same time, for half-filled even N wires Eq. (52) describes a dispersive branch of quasiparticle energies, which coincides with Eq. (50) under the condition $|\Delta(k_y)| \ll q(k_y)$.

For $\mu \neq 0$ the phase $\phi(k_{F,y})$ noticeably depends on $k_{F,y}$:

$$\phi(k_{F,y}) = k_{F,x} d(N+1) = (N+1)\cos^{-1}\left(-\frac{\mu}{q(k_{F,y})}\right). \quad (53)$$

Qualitative deviations of low-energy quasiparticle spectra, shown in Fig. 13, from the respective spectra of half-filled wires (see Figs. 10 and 11) are associated with the behavior of the phase $\phi(k_y)$. The odd-even effect in the spectra of (110) wires becomes less pronounced in the case of finite μ, as found by Ziegler *et al.*[13] For some values of μ the spectra of odd-N and even-N wires may have no qualitative differences at all. As it follows from Eq. (52) and, in a more general case, from Eq. (51), for $\mu \neq 0$ additional and strong dispersion of the spectra comes from the k_y dependence of the phase $\phi(k_{F,y})$. The larger the N, more oscillations of $\sin \phi(k_y)$ take place with varying the $k_{F,y}$. Hence, more extrema of $\omega_A(k_{F,y})$ arise. This results in additional peaks in the LDOS, which appear only in the presence of finite μ. As seen from Eq. (53), the phase ϕ can considerably vary, when the film (wire) thickness varies from Nd to $Nd-l$ and $a \ll l \ll \xi_0, l \ll Nd$. Thus, in averaging the spectrum over the film thickness, a large number of respective additional peaks arises, filling the whole low-energy band in the (110) wire with edges described by Eq. (52). This is in agreement with the quasiclassical results.[50,58]

The particle-hole asymmetry is another important feature of the spectra. It can be well pronounced for finite μ, but lies beyond the quasiclassical approximation. Figure 14 displays the asymmetric LDOS, calculated with Eq. (15) for (110) superconducting wires with $N=10$ and $N=11$ in the case $\mu=0.2t$. For comparison, the respective LDOS for $\mu=0$ is also shown. A well-pronounced peak at $\omega=-\mu$ arises with a deviation from half filling in the LDOS for the odd-N wires. We remind the reader that in the half-filled normal state (110) wires with odd N the dispersionless zero-energy quasiparticle states have been found in Sec. IV B 1 [see Eq. (30) with $\nu=(N+1)/2$]. The wave function of these states, as well as the residue of the polelike term in the Green's function, Eq. (33), is a standing wave across the wire, taking zero values on alternating sites. In the superconducting state the zero-energy standing wave disappears and the dispersionless zero-energy Andreev surface states arise. Their weight exponentially decays in the bulk of wide odd-N wires. In the presence of a deviation from half filling the energy of the quasiparticle states in the normal state odd-N wires shifts to $-\mu$. These dispersionless states with finite energy keep the character of standing waves. Further, in the superconducting wires with finite μ the low-energy states become dispersive both for odd- and even-N wires. As seen from Fig. 13 for the wire with $N=25$, the branch with lowest energy has in this case two extrema. The maximal value of $|\omega|$ for the states forming this branch, lies at $k_y=0$ and contributes to the peak at $\omega=-\mu$ associated with the hole contribution, if $\mu>0$. Since the order parameter vanishes at $k_y=0$, the respective quasiparticle wave function is a standing wave and the peak position coincides with that in the normal metal state of the wire. The minimal value of $|\omega|$ is zero and contributes to the zero-energy peak. The zero-energy peak is associated with comparatively large value of k_y, comparable with the size of the Brillouin zone, and the order parameter at this value of k_y is of order $\Delta_{\max}$. Thus, the zero-energy peak is associated with surface Andreev states, whose quasiparticle wave function decays in the bulk of wide odd-N wires. For narrow wires, the self-consistency condition becomes important. As shown in the following section, at finite μ the self-consistency condition can lead to more important consequences as compared with the case $\mu=0$.

V. SELF-CONSISTENT TREATMENT OF (110) WIRES

In previous sections, the order parameter was assumed constant over the whole width of the wire in order to allow for analytical solutions. Even for a single (110) surface, however, a self-consistent treatment of the order parameter gives rise to interesting effects: the $d_{x^2-y^2}$-wave order parameter is strongly suppressed near the surface and a complex *is*-admixture (or some other time-reversal symmetry-breaking state) is possible, which leads to a splitting of the zero-energy Andreev bound state.[17,18,22,24,33,34,39,59–64] Even larger effects are therefore to be expected for the wire limited by two (110) surfaces. Indeed, our self-consistent evaluation indicates that for very narrow wires a quasi-one-dimensional triplet superconducting state can replace the conventional $d_{x^2-y^2}+is$ state. For finite chemical potential μ the normal metal state can become energetically favorable as the ground state for narrow wires, while superconductivity recovers with increasing wire width. Under special conditions, even a mixture of singlet- and triplet-pairing can occur. It is important to recall at this point that one expects mean-field theory to break down as the one-dimensional (1D) limit is approached

even at $T=0$. Thus the predictions for various kinds of superconducting order mentioned below are to be treated with some skepticism as regards quantitative predictions. Nevertheless, we view our results as presenting intriguing evidence that when surface energies begin to become comparable to the energy differences between *d*-wave and other bulk pair channels, strong fluctuations with symmetries optimal for quasi-1D system, including spin-triplet pair fluctuations, will result.

A. Order parameter

Self-consistent solutions to Hamiltonian (1) were obtained by solving the Bogoliubov–de Gennes equations for (110) wires,

$$\begin{pmatrix} \xi_{k_y} & \Delta_{k_y} \\ \Delta^*_{-k_y} & -\xi_{k_y} \end{pmatrix} \begin{pmatrix} u_{k_y\lambda} \\ v_{k_y\lambda} \end{pmatrix} = E_{k_y\lambda} \begin{pmatrix} u_{k_y\lambda} \\ v_{k_y\lambda} \end{pmatrix}, \tag{54}$$

where $E_{k_y\lambda}$ with $\lambda=1,\ldots,N$ are the eigenvalues of the Bogoliubov–de Gennes equations and its eigenvectors $u_{k_y\lambda}(n)$ and $v_{k_y\lambda}(n)$ are the coefficients of the Bogoliubov transformation:

$$c_{k_y n\uparrow} = \sum_\lambda \{\gamma_{k_y\lambda\uparrow} u_{k_y\lambda}(n) - \gamma^\dagger_{k_y\lambda\downarrow} v^*_{k_y\lambda}(n)\},$$

$$c^\dagger_{-k_y n\downarrow} = \sum_\lambda \{\gamma_{k_y\lambda\uparrow} v_{k_y\lambda}(n) + \gamma^\dagger_{k_y\lambda\downarrow} u^*_{k_y\lambda}(n)\}. \tag{55}$$

Furthermore, ξ_{k_y} and Δ_{k_y} are matrices in the N layers of the (110) wire, i.e., the layers in x direction, and are given by (for notation see Fig. 7):

$$(\xi_{k_y})_{nn'} = -2t\cos k_y(\delta_{n'n+1} + \delta_{n'n-1}) - \mu\delta_{n'n},$$

$$(\Delta_{k_y})_{nn'} = (\Delta^+_{nn'} e^{-ik_y} + \Delta^-_{nn'} e^{ik_y})\delta_{n'n+1} + (\Delta^-_{nn'} e^{-ik_y} + \Delta^+_{nn'} e^{ik_y})\delta_{n'n-1}. \tag{56}$$

The gap values are determined by the following self-consistency equations:

$$\Delta^\pm_{nn+1} = -V\frac{1}{N}\sum_{k_y} e^{\pm ik_y}\langle c_{-k_y n+1\downarrow} c_{k_y n\uparrow}\rangle = V\frac{1}{N}\sum_{k_y}\sum_\lambda e^{\pm ik_y} u_{k_y\lambda}(n+1) v^*_{k_y\lambda}(n). \tag{57}$$

To simplify the numerical evaluation of the Bogoliubov–de Gennes equations we consider isolated wires here. For a Hamiltonian on a discrete lattice like that of Eq. (1), an isolated wire is equivalent to a wire limited by lines of unitary impurities, which is the boundary condition used for the analytical calculations in the previous sections.

For narrow wires we find a variety of different phases. The resulting phase diagram for a nearest-neighbor interaction strength of $V=1.1575t$, which gives rise to a gap of $\Delta_0=0.2t$ in a bulk system at $\mu=0$, is displayed in Fig. 15. For wires with widths up to $N=9$ we find a new phase over a wide range of chemical potentials characterized by $\Delta_{ij}=-\Delta_{ji}$ [stars in Figs. 15(c) and 15(d)], which is a signature of triplet pairing with $S_z=0$, the only triplet component compatible with Hamiltonian (1). For $\mu=0$ the amplitude of Δ_{ij} oscillates across the wire between zero and its maximum value [see Fig. 16(a)], indicating a one-dimensional nature of these new triplet-superconducting correlations [see Fig. 16(b)]. Although the oscillating behavior of Δ_{ij} remains for finite μ, its amplitude no longer vanishes exactly on alternating layers. Thus the strict one-dimensionality of the superconducting correlations seems to be a feature peculiar to $\mu=0$. This new triplet superconducting phase will be discussed in more detail below. At first we will focus on the singlet superconducting phase with possible $d_{x^2-y^2}$- and *s*-wave order parameters.

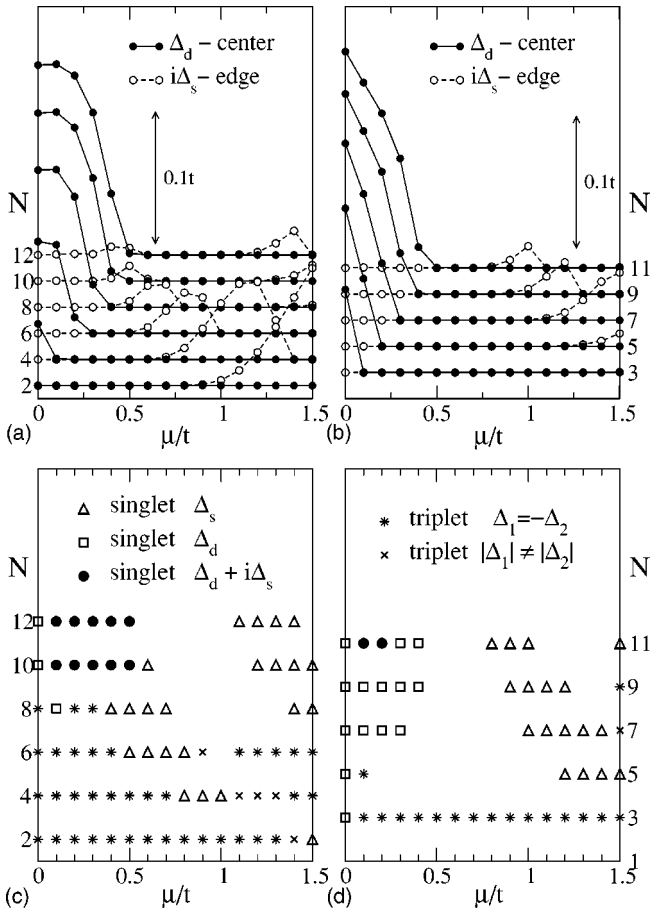

FIG. 15. Narrow wires with a nearest-neighbor interaction strength of $V=1.1575t$, which gives rise to a gap value of $\Delta_0=0.2t$ for the bulk system at $\mu=0$. Lower panels: phase diagram of the wires with even width (c) and with odd width (d). White space denotes $\Delta=0$, i.e., the normal state. Upper panels: corresponding amplitudes of the $d_{x^2-y^2}$ and *is*-order parameters displaying the value in the center of the wire for the $d_{x^2-y^2}$-wave case and the value at the edge of the wire in the *s*-wave case. These are the positions where the largest values of the respective order parameters are expected in the usual $d_{x^2-y^2}+is$ state.

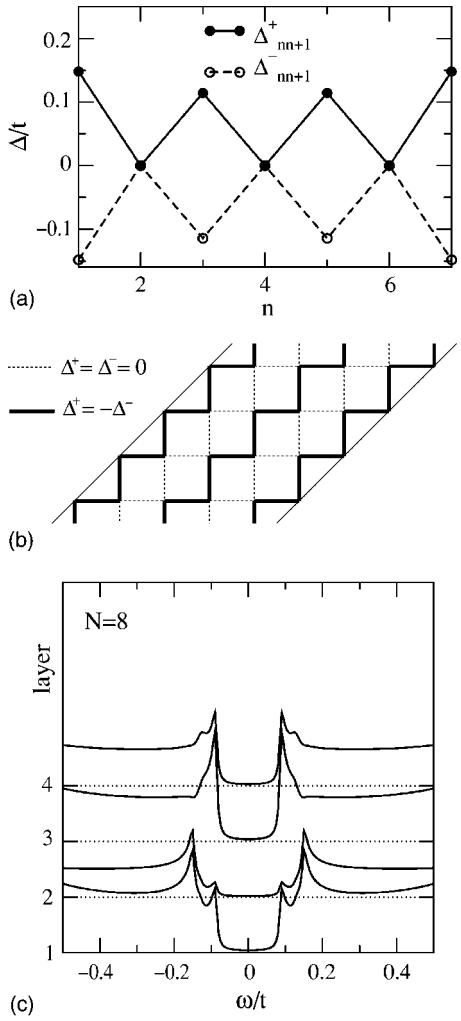

FIG. 16. Quasi-one-dimensional triplet superconducting state for $N=8$ and $\mu=0$. (a) Bond gap values $\Delta^{\pm}_{nn+1}$ [for definition see Eq. (58)] across the wire. (b) Illustration of the one-dimensional structure of the superconducting correlations for an $N=6$-(110) wire at $\mu=0$. (c) Density of states starting from the outermost layer of the wire up to the middle layer of the wire, where for illustrational purposes each layer has been shifted by an additional offset of $0.3t$.

Although we do not understand all details of the variability of the phase diagram, a few general trends seem clear. The larger the width of the wire the more of the usual $d_{x^2-y^2}+is$ phase [filled circles in Figs. 15(c) and 15(d)] is recovered. The corresponding amplitudes of the $d_{x^2-y^2}$- and *is* components of the order parameter are displayed in the upper panels of Fig. 15. For narrow wires the amplitude of the $d_{x^2-y^2}$-wave order parameter is finite only for small chemical potentials μ and a pure *s*-wave phase is favorable for large μ. These two phases are separated by a normal state region. For larger wire widths the range of the $d_{x^2-y^2}$-wave phase and the amplitude of the $d_{x^2-y^2}$-wave order parameter increase. The amplitude of the *s*-wave order parameter, on the other hand, decreases and the *s*-wave phase moves towards smaller chemical potentials until it merges with the $d_{x^2-y^2}$-wave phase, thereby giving rise to a finite *is* admixture near the edges of the wire, as expected in analogy to a single (110) surface.

The dependence of the amplitude of the $d_{x^2-y^2}$-wave order parameter on the width N of the wire is shown in Fig. 17. The upper panels refer to an interaction strength of $V=1.1575t$, which gives rise to a gap of $\Delta_0=0.2t$ for the bulk system at $\mu=0$. For $\mu=0$ we observe an even-odd oscillation in the amplitude of the order parameter [see Fig. 17(a)], which disappears for larger chemical potentials. The effect of finite μ on the suppression of the $d_{x^2-y^2}$-wave order parameter is considerably stronger in narrow wires than in the bulk system. For $\mu/t=0.4$ the $d_{x^2-y^2}$-wave order parameter vanishes for $N<10$ [squares in Fig. 17(a)], although the bulk gap is only reduced by a factor of approximately 0.8 [see Fig. 17(c)]. The dramatic suppression of the $d_{x^2-y^2}$-wave order parameter for finite μ is reduced upon consideration of larger nearest-neighbor interaction strengths, as can be seen in the lower panels of Fig. 17. For a larger interaction strength of $V=1.7682t$, which gives rise to a bulk gap value of $\Delta_0=0.4t$ at $\mu=0$, a pronounced even-odd effect remains at $\mu/t=0.4$ [see Fig. 17(d)] and the amplitude in the center of an $N=12$ wire is already very close to the bulk value [see Fig. 17(f)], contrary to the smaller interaction strength, where the amplitude in the center of an $N=12$ wire is still suppressed by a factor of more than 3 with respect to the bulk value [see Fig. 17(c)].

The emergence of a new triplet-superconducting phase for very narrow wires can be most easily understood by considering the smallest wire, i.e., the $N=2$ wire. Although the effect of fluctuations will be larger for smaller wires, we focus only on possible solutions of the BCS mean-field Hamiltonian (1) in the present paper. Inspection of the phase diagram of Fig. 15 shows that the *d*-wave order parameter vanishes for the $N=2$ wire. To investigate alternative ways in which the $N=2$ wire could lower its ground-state energy, we map it to a 1D chain (see Fig. 18). Although the gap values Δ_{ij} and Δ_{ji} could in principle differ in amplitude and by a phase factor ϕ, we restrict our treatment to $\phi=0$ and $\phi=\pi$. Note that $\phi=0$ corresponds to a singlet pairing state, whereas $\phi=\pi$ is a triplet pairing state with $S_z=0$.[65] To investigate the possibility of triplet superconductivity in these systems in more generality, one should retain pairing correlations with $S_z=\pm 1$ in the mean-field Hamiltonian as well. For now, however, we are satisfied with the observation that even for the simple nearest-neighbor pairing Hamiltonian (1) a triplet order parameter can be favored over a singlet order parameter in narrow geometries.

After Fourier transformation Hamiltonian (1) for the 1D chain reads

$$H_{\mathrm{MF}} = -\sum_{k\sigma}(2t\cos kd+\mu)c^{\dagger}_{k\sigma}c_{k\sigma} + \sum_{k}\{(\Delta_1 e^{ikd}+\Delta_2 e^{-ikd})c^{\dagger}_{-k\downarrow}c^{\dagger}_{k\uparrow}+\mathrm{H.c.}\}, \qquad (58)$$

where $\Delta_{ii+1}=-V\langle c_{i+1\downarrow}c_{i\uparrow}\rangle=\Delta_1$ and $\Delta_{i+1i}=-V\langle c_{i\downarrow}c_{i+1\uparrow}\rangle=\Delta_2$. It can be easily diagonalized using the Bogoliubov transformation to give a quasiparticle dispersion of

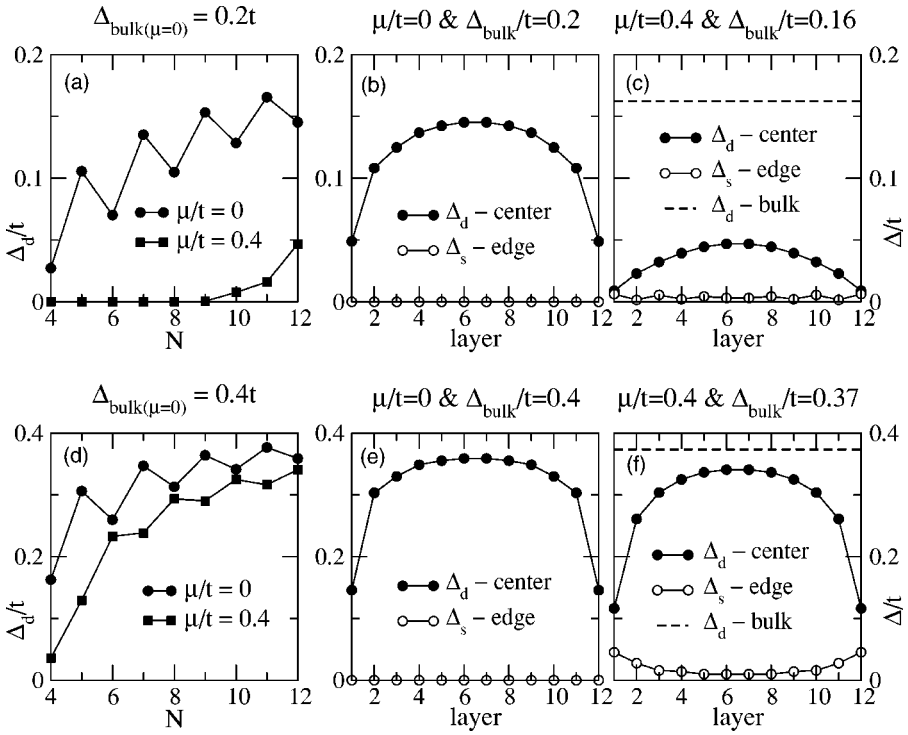

FIG. 17. Evolution of the $d_{x^2-y^2}$-wave order parameter with increasing wire width for two different interaction strengths $V=1.1575t$ (upper panels) and $V=1.7682t$ (lower panels), which give rise to a gap value of $\Delta_0=0.2t$ and $\Delta_0=0.4t$ for the bulk system at $\mu=0$, respectively. The first column displays the amplitude of the $d_{x^2-y^2}$ order parameter as a function of the wire width for two different chemical potentials $\mu/t=0$ and $\mu/t=0.4$. The other two columns show the variation of the $d_{x^2-y^2}$- and *is* component of the order parameter across the wire for $\mu/t=0$ (center column) and $\mu/t=0.4$ (right column). For comparison the reduced magnitude of the bulk order parameter at $\mu/t=0.4$ is displayed with dashed lines in the right panels.

$$E_k=\sqrt{\epsilon_k^2+\Delta_k^2},$$

$$\text{with } \epsilon_k=\frac{q(k)}{2}+\mu=2t\cos kd+\mu,$$

$$\Delta_k^2=\Delta_1^2+\Delta_2^2+2\Delta_1\Delta_2\cos 2kd, \tag{59}$$

where the gap values are to be determined from the following self-consistency equations:

$$\Delta_1=-V\frac{1}{4\pi d}\int_{-\pi d}^{\pi d}dk\frac{\Delta_1+\Delta_2\cos 2kd}{E_k},$$

$$\Delta_2=-V\frac{1}{4\pi d}\int_{-\pi d}^{\pi d}dk\frac{\Delta_1\cos 2kd+\Delta_2}{E_k}. \tag{60}$$

Four different phases emerge from this model by variation of the chemical potential μ and the nearest-neighbor interaction strength V (see Fig. 19). Below a critical interaction strength the order parameter vanishes and the normal state is the ground state of the 1D chain. For intermediate interaction strengths and small chemical potentials we find $\Delta_1=-\Delta_2$, i.e., a pure triplet superconducting state, whereas for large chemical potentials the ground state is characterized by $\Delta_1=\Delta_2$, i.e., a singlet extended *s*-wave state. In the singlet state the gap function is $\Delta_k\sim\cos kd$, i.e., it has nodes at $kd=\pm\pi/2$ whereas the triplet state gap function is $\Delta_k\sim\sin kd$, and therefore is maximum at $kd=\pm\pi/2$. This explains why the triplet state is favored over the singlet state for $\mu=0$, where the Fermi surface of the nearest-neighbor tight-binding model is at $kd=\pm\pi/2$. For larger chemical potentials the situation is reversed and the singlet extended *s*-wave state becomes more favorable than the triplet state. For large interaction strengths, we find different magnitudes for Δ_1 and Δ_2, which corresponds to a mixture of singlet and triplet pairing. In the limit $V\to\infty$, either of the gap values Δ_1 and Δ_2 approaches zero whereas the other goes to infinity, corresponding to an admixture of triplet and singlet order parameters with equal amplitudes.

With the phase diagram of the 1D chain in mind we are now able to better understand the phase diagram of narrow wires as displayed in Fig. 15. For small μ the new phase with $\Delta_{ij}=-\Delta_{ji}$ simply arises from the formation of quasi-one-dimensional triplet-superconducting correlations along $N=2$

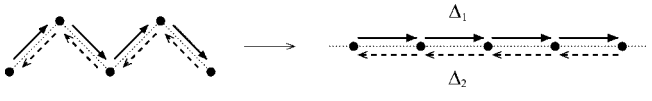

FIG. 18. Mapping of the $N=2$ wire with (110) orientation to the 1D chain with lattice constant d. Note that $\Delta_2=-\Delta_1$ corresponds to a triplet pairing state with $S_z=0$.

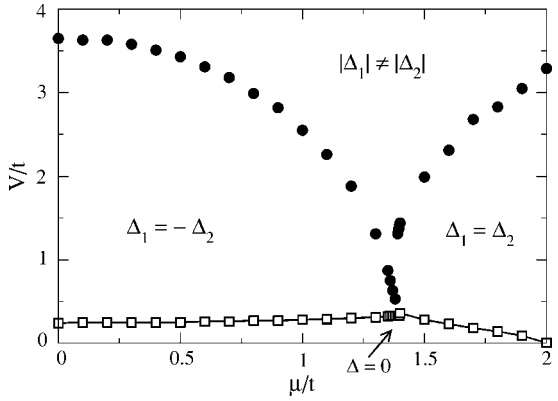

FIG. 19. Phase diagram for 1D chain as a function of chemical potential μ/t and nearest-neighbor interaction V/t.

wires [see Figs. 16(a) and 16(b)]. This also explains why this new phase is more favorable for wires with even width than with odd width (compare left and right panels in Fig. 15), as only the former can be divided evenly into $N=2$ wires. Note that also for the narrow wires, a critical coupling strength of similar magnitude as in the 1D chain is necessary to induce the triplet-superconducting state, which is, however, smaller than the interaction strength considered in this paper. At larger chemical potentials we find an extended *s*-wave order parameter analogous to the one-dimensional chain. More difficult to reconcile with the phase diagram of the one-dimensional chain, however, are the seemingly arbitrarily distributed mixtures of singlet- and triplet-superconducting order parameters (crosses in Fig. 15). The normal state regions, which occur for narrow wires and intermediate chemical potentials in Fig. 15, reflect the fact that superconductivity becomes less favorable in finite geometries and a critical coupling strength is necessary to induce it.[50]

B. Density of states

What does the phase diagram in Fig. 15 imply about the possible existence of Andreev bound states in narrow wires? In Fig. 16(c) the local density of states and the variation of the order parameter throughout the wire is depicted for the quasi-one-dimensional triplet superconducting state using the $N=8$ wires at $\mu=0$ as an example. Obviously, the density of states in this state is fully gapped, in analogy to the one-dimensional chain, and there are no Andreev bound states.

Close to half filling, for wider wire widths, the results are more conventional and the effects of self-consistency much simpler. In Fig. 20 the local density of states is displayed for the $N=10$ and the $N=11$ wires at $\mu=0$, which are characterized by a pure $d_{x^2-y^2}$ order parameter. Here, the main difference between the self-consistent (lower panels of Fig. 20) and the non-self-consistent results (upper panels of Fig. 20) is the suppression of the magnitude of the *d*-wave order parameter especially towards the edges of the wire (see also insets of Fig. 20). Whereas the weight of the zero-energy peak is reduced in the even-width ($N=10$) wire the weight of the zero-energy state in the odd-width wire ($N=11$) is hardly affected.

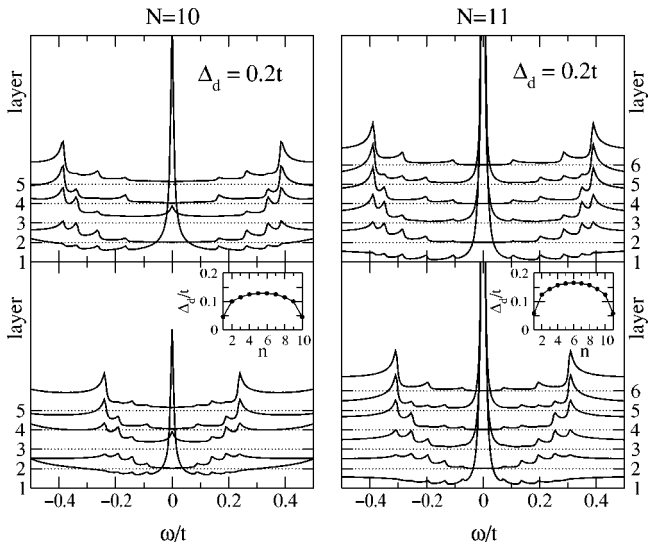

FIG. 20. Density of states for the $N=10$ wire (left panels) and the $N=11$ wire (right panels). Upper panels show the non-self-consistent results assuming a constant $d_{x^2-y^2}$ order parameter of $\Delta_0=0.2t$, whereas the lower panels display the density of states resulting from the self-consistently determined values of the *d*-wave order parameter, whose variation throughout the wire is depicted in the insets. All panels show the density of states starting from the outermost layer of the wire up to the middle layer of the wire, where for each layer towards the center of the wire an additional offset of $0.3t$ has been used.

VI. CONCLUSION

Motivated by recent scanning tunneling experiments on the $Ba_2Sr_2CaCu_2O_8$ systems which reveal inhomogeneous electronic structure on the nanoscale, we have analyzed in detail the electronic structure of *d*-wave quantum wires. These wires exemplify the effects of a constrained geometry while still being simple enough to allow for analytical solutions. To impose a restricted geometry we use lines of impurities with infinite scattering strength, a method which allows to cut arbitrarily shaped objects out of the two-dimensional plane. In principle, it is straightforward to extend this method to investigate the effects of tunneling between neighboring grains by reducing the scattering strength of the impurities and thus lowering the potential barrier between neighboring grains.

New and interesting physics arises from interference effects between the two surfaces of the wire when its width is of the order of the superconducting coherence length. Contrary to *s*-wave superconductors in finite geometries, the surface pair breaking plays an important role. In this respect, the existence and nature of Andreev bound states in constricted geometry is of particular interest. In order to single out new effects peculiar to quantum wires and arising from the interference of the two surfaces, we have addressed the case of a single surface in the first part of the paper, concentrating on surfaces with (100), (210), and (110) orientations in a nearest-neighbor tight-binding model at half filling. Andreev bound states can form on surfaces with orientations deviating from the (100) direction due to the sign change of the *d*-wave order parameter. However, in the presence of several channels for reflection of quasiparticles from the surface, the zero-energy Andreev states may not exist, as is the case for the (210) surface of the square lattice. Here our results are in qualitative agreement with earlier work based either on the quasiclassical approximation or Bogoliubov–de Gennes equations. Only for the (110) surface, which involves the strongest pair breaking, do we find a zero-energy Andreev bound state, whose amplitude decreases with the square of the inverse distance from the surface and vanishes on even layers.

In the main part of this work, we focused on quantum wires with (110) orientation, which display a pronounced "width parity" effect. The special case of electrons hopping on a square lattice with half-filled tight-binding band was treated most extensively. For wires of this type with an odd

number of chains N only one subgap state, a dispersionless zero-energy Andreev bound state, exists. As in the single-surface case, the amplitude of the ZES vanishes on even layers and decays towards the center of the wire. In addition to the ZES, there are $N-1$ dispersive modes, which are doubly degenerate due to particle-hole symmetry and are not Andreev states.

In the case of even-N half-filled wires, a splitting of the branches occurs which is associated with a symmetry breaking $k_y \rightarrow -k_y$, and a total of $2N$ dispersive modes exist. Although there is no dispersionless ZES, all quasiparticle states in the even width wire are of Andreev character in the sense that the current of the probability density vanishes due to opposite contributions from particle and hole excitations. These quasiparticles occupy either conventional Andreev-type surface states or a new type of Andreev standing wave, according to their momentum k_y parallel to the wire. In the 2D limit $N \rightarrow \infty$, the lowest energy dispersive state was shown to transform into the usual zero-energy Andreev bound state at the impenetrable surface, while the standing wave states evolve into either the continuous spectrum or the surface states. With increasing deviation from half-filling, odd-even effects in the wires become less pronounced. The evolution of the Fermi-surface shape with these deviations can result in additional extrema in the quasiparticle dispersive modes and, hence, new peaks in the LDOS. Large-scale faceting of the surfaces with characteristic scales larger than the wire thickness will not influence our results significantly. However, small-scale inhomogeneities such as pointlike defects and impurities can substantially change the effects of interference induced by wire surfaces, even if the phase breaking length is large.

The small coherence length of high-temperature superconductors leads to further restrictions on the applicability of the quasiclassical results to superconducting wires or films, whose width is less than or comparable to the coherence length. For narrow wires of (110) orientation, the self-consistent treatment of the order parameter is found to have a large effect. For wires with widths less than the superconducting coherence length (up to $N=9$ for the particular parameters used in our numerical calculations), especially for the even width wires, a new phase characterized by quasi-one-dimensional triplet pairing is found in the mean-field phase diagram. This new phase is fully gapped and characterized by the absence of Andreev bound states. The larger the width of the strip, the more the $d+is$ state, which is expected for a single surface with (110) orientation, dominates the phase diagram near half filling. With respect to the density of states at half filling, where the order parameter has only a d-wave component, the main effect of the self-consistent treatment is the suppression of the magnitude of the d-wave order parameter, especially near the surfaces of the wire.

It is interesting to end this discussion with some speculations on the role of bound quasiparticle states and edge effects of this type on the spectra of weakly coupled superconducting grains as apparently observed in STM experiments. Such irregular grains should contain nanoscale "facets" at all possible angles, so presumably the most general situation with sizable particle-hole asymmetry and mixture of even- and odd-N boundary conditions will apply. If we first assume that the pair interaction and grain size are such that one may ignore the triplet states found in the self-consistent treatment, we expect the spectra of weakly coupled grains to be dominated by the zero-dimensional analogs of the dispersive subgap states discussed here, i.e., there should be a wide distribution of bound-state energies depending on local geometry of the grain, and visible in the LDOS as measured by STM. In this sense we question whether the weakly coupled grain picture is, in fact, applicable to the experiments in question, which appear to see a very *homogeneous* spectrum at low energies in the superconducting state.

A second remark is based on our observation that in nanoscale confined geometry, spin-triplet fluctuations may become more favorable. Such time-reversal symmetry breaking fluctuations will clearly lead to local spontaneous currents, an issue which has recently been raised again in angle-resolved photoemission studies.[66] Future studies of small grains are planned to address these issues.

ACKNOWLEDGMENTS

We thank I. Bobkova, Ya. Fominov, T. Kopp, J. Mannhart, and K. Ziegler for useful discussions. This work was supported, in part, by Grant No. RFBR 02-02-16643 (A.M.B. and Yu.S.B.) and No. NSF-INT-0340536 (P.J.H. and Yu.S.B). A.M.B. acknowledges the support of Dynasty Foundation and T.S.N. acknowledges the support of the Alexander von Humboldt Foundation.

[1] H. F. Hess, R. B. Robinson, R. C. Dynes, J. M. Valles, and J. V. Waszak, Phys. Rev. Lett. **62**, 214 (1989).

[2] I. Maggio-Aprile, Ch. Renner, A. Erb, E. Walker, and Ø. Fischer, Phys. Rev. Lett. **75**, 2754 (1995).

[3] Ali Yazdani, C. M. Howald, C. P. Lutz, A. Kapitulnik, and D. M. Eigler, Phys. Rev. Lett. **83**, 176 (1999).

[4] E. W. Hudson, S. H. Pan, A. K. Gupta, K.-W. Ng, and J. C. Davis, Science **285**, 88 (1999).

[5] S. H. Pan, E. W. Hudson, K. M. Lang, H. Eisaki, S. Uchida, and J. C. Davis, Nature (London) **403**, 746 (2000).

[6] T. Cren *et al.*, Phys. Rev. Lett. **84**, 147 (2000).

[7] S.-H. Pan *et al.*, Nature (London) **413**, 282 (2001).

[8] D. J. Derro, E. W. Hudson, K. M. Lang, S. H. Pan, J. C. Davis, J. T. Markert, and A. L. de Lozanne, Phys. Rev. Lett. **88**, 097002 (2002).

[9] C. Howald *et al.*, Phys. Rev. B **64**, 100504 (2001).

[10] K. M. Lang *et al.*, Nature (London) **415**, 412 (2002).

[11] J. von Delft and D. C. Ralph, Phys. Rep. **345**, 61 (2001).

[12] C. N. Lau, N. Markovic, M. Bockrath, A. Bezryadin, and M. Tinkham, Phys. Rev. Lett. **87**, 217003 (2001).

[13] K. Ziegler, W. A. Atkinson, and P. J. Hirschfeld, Phys. Rev. B **64**, 054512 (2001).
[14] J. Geerk, X. Xi, and G. Linker, Z. Phys. B: Condens. Matter **73**, 329 (1988).
[15] C.-R. Hu, Phys. Rev. Lett. **72**, 1526 (1994).
[16] Y. Tanaka and S. Kashiwaya, Phys. Rev. Lett. **74**, 3451 (1995).
[17] M. Matsumoto and H. Shiba, J. Phys. Soc. Jpn. **64**, 1703 (1995); **64**, 3384 (1995); **64**, 4867 (1995); **65**, 2194 (1996).
[18] L. J. Buchholtz, M. Palumbo, D. Rainer, and J. A. Sauls, J. Low Temp. Phys. **101**, 1079 (1995); **101**, 1099 (1995).
[19] S. Kashiwaya, Y. Tanaka, M. Koyanagi, H. Takashima, and K. Kajumura, Phys. Rev. B **51**, 1350 (1995).
[20] M. Covington, R. Scheuerer, K. Bloom, and L. H. Greene, Appl. Phys. Lett. **68**, 1717 (1996).
[21] J. H. Xu, J. H. Miller, Jr., and C. S. Ting, Phys. Rev. B **53**, 3604 (1996).
[22] M. Fogelström, D. Rainer, and J. A. Sauls, Phys. Rev. Lett. **79**, 281 (1997).
[23] Yu. Barash, H. Burkhardt, and A. Svidzinsky, Phys. Rev. B **55**, 15 282 (1997).
[24] M. Covington, M. Aprili, E. Paraoanu, L. H. Greene, F. Xu, J. Zhu, and C. A. Mirkin, Phys. Rev. Lett. **79**, 277 (1997).
[25] L. Alff, H. Takashima, S. Kashiwaya, N. Terada, H. Ihara, Y. Tanaka, M. Koyanagi, and K. Kajimura, Phys. Rev. B **55**, R14 757 (1997).
[26] J. W. Ekin, Y. Xu, S. Mao, T. Venkatesan, D. W. Face, M. Eddy, and S. A. Wolf, Phys. Rev. B **56**, 13 746 (1997).
[27] M. Aprili, M. Covington, E. Paraoanu, B. Niedermeier, and L. H. Greene, Phys. Rev. B **57**, R8139 (1998).
[28] L. Alff, S. Kleefisch, U. Schoop, M. Zittartz, T. Kemen, T. Bauch, A. Marx, and R. Gross, Eur. Phys. J. B **5**, 423 (1998).
[29] L. Alff, A. Beck, R. Gross, A. Marx, S. Kleefisch, Th. Bauch, H. Sato, M. Naito, and G. Koren, Phys. Rev. B **58**, 11 197 (1998).
[30] S. Sinha and K.-W. Ng, Phys. Rev. Lett. **80**, 1296 (1998).
[31] J. Y. T. Wei, N.-C. Yeh, D. F. Garrigus, and M. Strasik, Phys. Rev. Lett. **81**, 2542 (1998).
[32] M. Aprili, E. Badica, and L. H. Green, Phys. Rev. Lett. **83**, 4630 (1999).
[33] R. Krupke and G. Deutscher, Phys. Rev. Lett. **83**, 4634 (1999).
[34] J.-X. Zhu, B. Friedman, and C. S. Ting, Phys. Rev. B **59**, 3353 (1999).
[35] M. Covington and L. H. Green, Phys. Rev. B **62**, 12 440 (2000).
[36] P. Pairor and M. B. Walker, Phys. Rev. B **65**, 064507 (2002).
[37] H. Aubin, L. H. Greene, Sha Jian, and D. G. Hinks, Phys. Rev. Lett. **89**, 177001 (2002).
[38] Shin-Tza Wu and Chung-Yu Mou, Phys. Rev. B **67**, 024503 (2003).
[39] L. H. Green, P. Hentges, H. Aubin, M. Aprili, E. Badica, M. Covington, M. M. Pafford, G. Westwood, W. G. Klemperer, S. Jian, and D. G. Hinks, Physica C **387**, 162 (2003).
[40] Y. Tanaka and S. Kashiwaya, Phys. Rev. B **53**, 11 957 (1996).
[41] Yu. S. Barash, H. Burkhardt, and D. Rainer, Phys. Rev. Lett. **77**, 4070 (1996).
[42] E. Il'ichev *et al.*, Phys. Rev. Lett. **86**, 5369 (2001).
[43] G. Testa, A. Monaco, E. Esposito, E. Sarnelli, D.-J. Kang, E. J. Tarte, S. H. Mennema, and M. G. Blamire, cond-mat/0310727 (unpublished).
[44] H. Walter, W. Prusseit, R. Semerad, H. Kinder, W. Assmann, H. Huber, H. Burkhardt, D. Rainer, and J. A. Sauls, Phys. Rev. Lett. **80**, 3598 (1998).
[45] Yu. S. Barash, M. S. Kalenkov, and J. Kurkijärvi, Phys. Rev. B **62**, 6665 (2000).
[46] A. Carrington, F. Manzano, R. Prozorov, R. W. Giannetta, N. Kameda, and T. Tamegai, Phys. Rev. Lett. **86**, 1074 (2001).
[47] S. Kashiwaya and Y. Tanaka, Rep. Prog. Phys. **63**, 1641 (2000).
[48] T. Löfwander, V. S. Shumeiko, and G. Wendin, Supercond. Sci. Technol. **14**, R53 (2001).
[49] F. J. Giessibl, Rev. Mod. Phys. **75**, 949 (2003).
[50] Y. Nagato and K. Nagai, Phys. Rev. B **51**, 16 254 (1995).
[51] M. B. Walker and P. Pairor, Phys. Rev. B **59**, 1421 (1999).
[52] Y. N. Joglekar, A. H. Castro Neto, and A. V. Balatsky, Phys. Rev. Lett. **92**, 037004 (2004).
[53] D. K. Morr and E. Demler, cond-mat/0010460 (unpublished).
[54] I. Tamm, Phys. Z. Sowjetunion **1**, 733 (1932).
[55] V. L. Ginzburg and D. A. Kirzhnits, Zh. Eksp. Teor. Fiz. **46**, 397 (1964) [Sov. Phys. JETP **19**, 269 (1964)].
[56] V. F. Gantmakher and Y. B. Levinson, *Carrier Scattering in Metals and Semiconductors*, Modern Problems in Condensed Matter Sciences Vol. 19 (Elsevier Science, Amsterdam, 1987).
[57] In the presence of half-filling, surfaces with (110) orientations represent a special case for the square lattice, since the parallel component of the Fermi momentum coincides in this case with the edge of the surface-adapted Brillouin zone. In the problems in question the role of the edge of the Brillouin zone becomes quite important, in particular, for this reason. In a more general case one can expect that extrema of the quasiparticle spectra would arise at other values of the momentum component parallel to the surface, which are comparable with the scale of the Brillouin zone.
[58] Ya. V. Fominov and A. A. Golubov, cond-mat/0402381 (unpublished).
[59] S. Kos, Phys. Rev. B **63**, 214506 (2001).
[60] C. Honerkamp, K. Wakabayashi, and M. Sigrist, Europhys. Lett. **50**, 368 (2000).
[61] Y. Ohashi, Phys. Rev. B **60**, 15 388 (1999).
[62] W. K. Neils and D. J. Van Harlingen, Phys. Rev. Lett. **88**, 047001 (2002).
[63] A. Sharoni, O. Millo, A. Koren, Y. Dagan, R. Beck, G. Deutscher, and G. Koren, Phys. Rev. B **65**, 134526 (2002).
[64] A. Kohen, G. Leibovitch, and G. Deutscher, Phys. Rev. Lett. **90**, 207005 (2003).
[65] In terms of standard representation of singlet and triplet pairings $\hat{\Delta}_s = \Delta i\hat{\sigma}_2, \hat{\Delta}_t = (\mathbf{d}\cdot\hat{\boldsymbol{\sigma}})i\hat{\sigma}_2$, one finds for the order parameters we introduced $\Delta_1 = \Delta + d_z, \Delta_2 = \Delta - d_z, d_x = d_y = 0$. Hence, in the purely singlet case $\Delta_1 = \Delta_2$, while for the triplet pairing $\Delta_1 = -\Delta_2$. Otherwise, there is a mixture of singlet and triplet pairings.
[66] A. Kaminski, S. Rosenknanz, H. M. Fretwell, J. C. Campuzano, Z. Li, H. Raffy, W. G. Cullen, H. You, C. G. Olson, and C. M. Varma, Nature (London) **416**, 610 (2002).